Transportation Research Part E

Vessel Routing Optimization for Floating Macro-Marine Debris Collection in the Ocean Considering Dynamic Velocity and Direction

--Manuscript Draft--

Manuscript Number:	TRE-D-20-01338
Article Type:	Full Length Article
Keywords:	Marine debris; vessel routing problem; vessel velocity and direction; ocean currents and winds; branch-and-cut; adaptive large neighborhood search.
Corresponding Author:	Junfeng Ma, Ph.D. Mississippi State University Starkville, UNITED STATES
First Author:	Gang Duan, Ph.d.
Order of Authors:	Gang Duan, Ph.d.
	Amin Aghalari
	Li Chen, Ph.d.
	Mohammad Marufuzzaman, Ph.d.
	Junfeng Ma, Ph.D.
Abstract:	Floating macro-marine debris becomes a global environmental problem when emitted into the ocean. It damages the marine ecosystem, threatens human health, and also causes incalculable economic losses. To effectively mitigate the risk, we propose the vessel routing optimization with a time window to collect and remove marine debris. Ocean currents and winds can transport debris and also affect the velocity and direction of the collecting vessel. We first employ GNOME software to predict the trajectory of debris and set a time window for each debris location. A mixed-integer nonlinear programming with vessel velocity consideration model is proposed to minimize the total debris collection cost. We propose two customized solution approaches: Branch-and-Cut (B&C) algorithm and two-stage Adaptive Large Neighborhood Search (ALNS) based heuristic algorithm to solve the proposed mathematical model in a reasonable timeframe. A computational study in the vicinity of Boston is used to validate the proposed model and the solution algorithms. The result indicates that the average optimality gap for GUROBI and B&C algorithm is 17.53% and 10.52%, respectively, while this gap is only 3.44% for the ALNS algorithm. Moreover, the average computing time of the ALNS algorithm is roughly 24 and 17 times faster than that of the GUROBI and the B&C algorithm, respectively. The experimental results show that distance from debris location to the harbor is positively related to the collection cost and negatively related to the average usage of vessels' capacity, and the dispersion of debris is also positively related to the fuel consumption of vessels.

Department of Industrial and Systems Engineering,
Mississippi State University, Mississippi State,
MS 39762, USA

Dear Editor and Reviewers:

Here within enclosed is our paper for consideration to be published on "***Transportation Research Part E: Logistics and Transportation Review***". The further information about the paper is in the following:
The Title: **Vessel Routing Optimization for Floating Macro-Marine Debris Collection in the Ocean Considering Dynamic Velocity and Direction**

The Authors: Gang Duan; Amin Aghalari; Li Chen; Mohammad Marufuzzaman; Junfeng Ma

We declare solemnly that, the paper to be submitted is our research achievements. As far as we know, except the text marked in particular and acknowledgments, the paper does not include other published or written achievements. All authors have read and approved this version of the article, and due care has been taken to ensure the integrity of the work. No part of this paper has been published or submitted elsewhere. No conflict of interest exists in the submission of this manuscript.

In this work, the aim of this paper is to collect floating macro-marine debris in the ocean. Ocean currents and winds can transport debris and also affect the velocity and direction of the collecting vessel. We first employ GNOME software to predict the trajectory of debris and set a time window for each debris location. A mixed-integer nonlinear programming with vessel velocity consideration model is proposed to minimize the total debris collection cost. We propose two customized solution approaches: Branch-and-Cut (B&C) algorithm and two-stage Adaptive Large Neighborhood Search (ALNS) based heuristic algorithm to solve the proposed mathematical model in a reasonable timeframe. A computational study in the vicinity of Boston is used to validate the proposed model and the solution algorithms. The experimental results show that distance from debris location to the harbor is positively related to the collection cost and negatively related to the average usage of vessels' capacity, and the dispersion of debris is also positively related to the fuel consumption of vessels.

We appreciate your consideration of our manuscript, and we look forward to receiving comments from the reviewers. Please let us know if you need any further information.

Sincerely yours,
Authors

Corresponding author:
Name: Junfeng Ma

E-mail: ma@ise.msstate.edu

Title Page (with Author Details)

Vessel Routing Optimization for Floating Macro-Marine Debris Collection in the Ocean Considering Dynamic Velocity and Direction

Gang Duan[1], Amin Aghalari[2], Li Chen[3], Mohammad Marufuzzaman[2], Junfeng Ma[2*]

1. School of Traffic and Transportation, Lanzhou Jiaotong University, Gansu, 730070, China;
2. Department of Industrial & Systems Engineering, Mississippi State University, Mississippi State, MS 39762, USA
3. Department of Mathematics, Lanzhou City University, Gansu, 730070, China.

Gang Duan, Email: duangang@mail.lzjtu.cn; Tel: +86 931-4938025

Amin Aghalari, Email: aa2683@msstate.edu

Li Chen, Email: lichen_79@163.com; Tel: +86 931-7601137

Mohammad Marufuzzaman, Email: maruf@ise.msstate.edu; Tel: +1 662-325-7216

[*]Junfeng Ma, corresponding author, Email: ma@ise.msstate.edu; Tel: +1 662-325-7625

Vessel Routing Optimization for Floating Macro-Marine Debris Collection in the Ocean Considering Dynamic Velocity and Direction

Abstract

Floating macro-marine debris becomes a global environmental problem when emitted into the ocean. It damages the marine ecosystem, threatens human health, and also causes incalculable economic losses. To effectively mitigate the risk, we propose the vessel routing optimization with a time window to collect and remove marine debris. Ocean currents and winds can transport debris and also affect the velocity and direction of the collecting vessel. We first employ GNOME software to predict the trajectory of debris and set a time window for each debris location. A mixed-integer nonlinear programming with vessel velocity consideration model is proposed to minimize the total debris collection cost. We propose two customized solution approaches: Branch-and-Cut (B&C) algorithm and two-stage Adaptive Large Neighborhood Search (ALNS) based heuristic algorithm to solve the proposed mathematical model in a reasonable timeframe. A computational study in the vicinity of Boston is used to validate the proposed model and the solution algorithms. The result indicates that the average optimality gap for GUROBI and B&C algorithm is 17.53% and 10.52%, respectively, while this gap is only 3.44% for the ALNS algorithm. Moreover, the average computing time of the ALNS algorithm is roughly 24 and 17 times faster than that of the GUROBI and the B&C algorithm, respectively. The experimental results show that distance from debris location to the harbor is positively related to the collection cost and negatively related to the average usage of vessels' capacity, and the dispersion of debris is also positively related to the fuel consumption of vessels.

Keywords: Marine debris; vessel routing problem; vessel velocity and direction; ocean currents and winds; branch-and-cut; adaptive large neighborhood search.

1. Introduction

Marine debris is defined as any persistent solid material that is manufactured or processed and directly or indirectly, intentionally or unintentionally, disposed of or abandoned into the marine environment or the Great Lakes. There are various types of marine debris, such as derelict vessels, abandoned fishing gears, and even microplastics less than 5 mm that are invisible to the naked eye (Yang et al., 2015; Zhang, 2017). Common rubbish on land, such as plastic products, metals, textiles, papers, and woodwares, found in the ocean can also be treated as marine debris. Nearly 80% of marine debris originates from land-based sources, and the rest comes from ocean-based sources (GESAMP, 2015). In this study, we focus on visable floating macro-marine debris, where debris locations would be changed along with currents and winds over time in the ocean.

When a piece of land-based debris enters the marine environment, it may be broken down into several small pieces and remain in the marine environment for a long time. The heavy parts will sink to the bottom of the sea, while the light ones will float in the sea. Some of the debris will be blown by winds to the shore or the beach, but more will move with the winds and ocean currents over time, gather in the deep sea, and eventually form huge garbage patches in the deep ocean. The largest garbage patch is the Great Pacific Garbage Patch located in the North Pacific Gyre, which shares the same size as Texas (Sigler, 2014). **Figure 1** shows the first global map of plastic marine debris created by Cózar et al. (2014). The five gray areas in **Figure 1** represent the five large gyres which contain the most debris (red dots). They also pointed out that there would be more debris in the ocean due to the intensification of human activities and nature influences such as winds, rain, and tsunami in the next decade. The recent survey of van Sebille et al. (2015) also supports this statement. As

plastic accounts for 75% of the marine debris (Barnes et al., 2009), most studies estimated the amount of marine debris by quantifying plastic debris. Most of the debris is harmful to the environment, marine creatures, human health, and the economy.

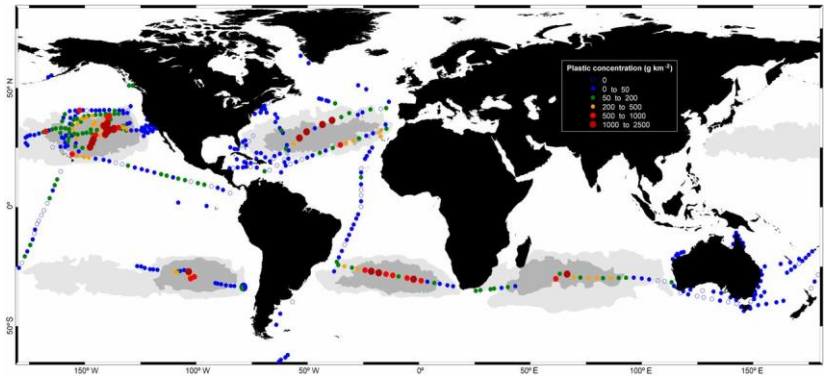

Figure 1 Densities of plastic debris in surface waters of the global ocean (Cózar et al., 2014)

This paper mainly focuses on the cleanup of offshore debris, which requires vessels dispatched to collect the debris in the ocean and then return to the harbor. Marine debris cleanup is different with land-based garbage collection mainly because of the impact of the meteorological conditions, such as winds and ocean currents. Marine debris locations will not be fixed in the sea and instead will continue to move over time. When the initial location of the debris is identified, it will be changed significantly over time under the influence of winds and ocean currents. The vessel cannot be dispatched immediately from a harbor (restricted by meteorological conditions or vessel availability), or the vessel arrives at the initial location after a period of time, which might result in less or even no debris will be captured at the original location. Therefore, the time window must be considered for debris locations. Moreover, because of the influence of winds and ocean currents, the velocity and direction of the vessel are different with those in still water. If we can take the advantages of winds and ocean currents, the vessel can not only save more fuels but reduce the travel time to the current debris location and complete the debris collection in the more economic way.

Our previous study first proposed a three-stage integrated framework to collect marine debris (Duan et al., 2020). The first stage is to use satellite imagery to determine the initial location of the debris; then, marine debris trajectory is tracked and predicted using GNOME [1] (General NOAA Operational Modeling Environment) software developed by the Emergency Response Division of NOAA's Office of Response and Restoration in the second stage; and the third stage develops and optimizes the vessel routing with time windows (VRPTWs) consideration to collect the marine debris. Although the vessel velocity was taken as a decision variable in the previous paper, the influence of winds and ocean currents on vessel velocity and direction was not considered. When a vessel travels in the ocean, it receives the combined action of winds and ocean currents, called resultant force. Thus, the velocity and direction of a vessel we observed on the ground are different with the actual velocity and direction of a vessel in the sea. Take vessel direction under the impact of ocean currents as an illustrative example in **Figure 2**. The vessel needs to reach to point *j* from a given point *i*. When the ocean surface is calm, the vessel will travel straight from point *i* to *j* along the line, as shown by the arrow direction in **Figure 2a**. When the direction of ocean currents is east, *iB* (red arrow direction), the vessel must travel along the blue

[1]Available from: http://response.restoration.noaa.gov/software/gnome/gnomeinfo.html

arrow direction, *iA*, in order to reach to point *j*, as shown in **Figure 2b**. The vessel direction we observed on the ground, black arrow direction *ij* shown in **Figure 2a**, is called the direction relative to the ground. The actual vessel direction in the ocean, blue arrow direction *iA* shown in **Figure 2b**, named the direction relative to the sea. Similarly, the vessel velocity is divided into two types, velocity relative to the ground and velocity relative to the sea.

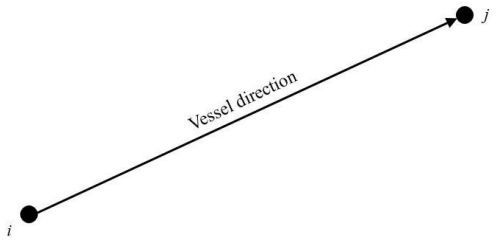

Figure 2a Vessel direction under sea calm

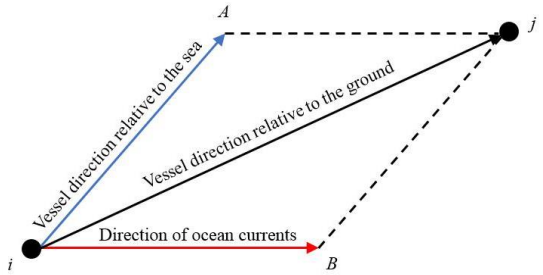

Figure 2b Vessel direction under ocean currents

Figure 2 Illustrative example of vessel direction

Based on the above-mentioned analysis, we model the marine debris collection problem as generalized VRPTWs under the consideration of winds and ocean currents. First of all, the GNOME software is used to predict and track the debris trajectory along with the time and the meteorological conditions. Then, a generalized VRPTWs for debris collection is modeled as a mixed-integer nonlinear programming model with an objective of minimizing the total collection cost, including fuel cost, port berth and unloading cost, vessel rent, vessel insurance, and labor cost, subject to vessel capacity of volume, weight, and fuel tank, vessel velocity, and time window at each debris location. The novelty in this paper locates on the one-to-one mapping between vessel velocity and direction relative to the sea, and vessel velocity and direction relative to the ground, under the influence of winds and ocean currents. With this one-to-one mapping, we assume velocity relative to the ground is a variable, and direction relative to the ground is constant in the generalized VRPTWs, which can significantly simplify the model. A Branch-and-Cut (B&C) algorithm and a two-stage heuristic algorithm, based on the Adaptive Large Neighborhood Search (ALNS) algorithm, are designed to solve the proposed problem with different scales.

The organization of the remainder is as follows. Section 2 provides a pertinent literature review, including a brief introduction of GNOME software. In section 3, we propose a mixed-integer nonlinear programming model for the generalized VRPTWs for debris collection. Section 4 designs a B&C algorithm and a two-stage heuristic algorithm to solve the proposed model. Section 5 reports the obtained analytical results by a case study in the vicinity of Boston. The conclusion and future directions are given in section 6.

2. Literature Review

2.1 Marine Debris

It is almost impossible to accurately estimate how much debris existed in the ocean. This is because 1) the ocean is too big to count debris everywhere; 2) the debris breaks down into several small pieces, some are too small to be detected, and some can be eaten by marine animals; and 3) there is no appropriate estimating method (Duan et al., 2020). Some prior studies have been conducted to investigate the impact, type, distribution, and source of marine debris. Schulz et al. (2019) defined baseline value and threshold value to assess the effect of beach debris management. The baseline value refers to the average of beach debris, while the threshold value is the lowest level of impact of beach debris on human sensory

discomfort. Angelini et al. (2019) and Lavers et al. (2016) examined the accuracy of the identification of beach debris and the factors that may affect such accuracy. Among all the subjective and objective factors, the color of debris is the most important factor to correctly identify debris. The results showed that blue debris has the highest recognition rate, close to 100%, while white and clear debris recognition rates are only half, so they are likely to be missed during beach debris cleanup. Peng et al. (2019) estimated the overall length of marine debris area is roughly 1,700-1,800 meters in the tributary submarine canyons of the Xisha Trough in the South China Sea.

A recent report showed that marine debris has negative impacts on more than 800 animal species in 2016, increasing from 663 to 817 since 2012 (Dias, 2016). One year later, this number has been increased to more than 1,300 (Bergmann et al., 2017). According to a study from the University of Southern California (California Ocean Science Trust, 2011), up to one million marine creatures are killed each year by marine debris. Some debris such as clear plastic bags, lighter, and bottle caps were eaten by marine creatures, including fish, seabirds, mammals, and invertebrates. These types of debris cannot be digested in the creatures' stomachs, causing them to feel full and stop eating, and eventually starving to death (Currie et al., 2017; Camedda et al., 2014). The discarded or abandoned fishing gear is known as "ghost fishing" as it will continue to fish even it is no longer used by fishermen (Marine Mammal Commission, 1998). Some debris such as plastic sheets and fishing lines can entangle in various body parts of animals, causing infection, inconvenience, amputation, and even death (Possatto et al., 2011; Mascarenhas et al., 2004; Bauer-Civiello et al., 2018).

Marine debris will also bring significant economic losses. According to the United Nations (2017), the damage of marine ecosystems caused by marine debris is worth at least $8 billion. The significantly increased beach debris leads to the reduction of visitors by 63 percent, from 890,435 to 330,207, and caused more than $29 million in tourist losses after a period of heavy rain in Geoje Island in 2011 (Jang et al., 2014). A survey of Cape Town residents showed that nearly half of visitors would like to pay seven times more than the average travel fee to visit a clean beach instead of visiting a local debris beach (Ballance et al., 2000). McIlgorm et al. (2011) proposed a marine waste recycling model to evaluate the cost and benefit of using biodegradable materials to reduce marine debris. Oosterhuis et al. (2014) discussed the economic instruments that can be used to reduce marine debris, such as environmental taxes on plastic bags, deposits for recycling empty bottles, tourist taxes on coastal areas, and incentives for fishing boats that clean up marine debris.

2.2 Waste Collection

The waste collection problem is considered to be one of the most difficult operational problems in the municipal sector, and it has attracted significant attentions (Huang & Lin, 2015; Alizadeh et al., 2019b). Markov et al. (2016) and Benjamin and Beasley (2010) studied multiple routings for one vehicle. Ramos et al. (2018) utilized sensors to monitor the filling status of the bins and send the data to the control center in the real-time. The vehicle routing is dynamically optimized based upon the status data of the bins. Bányai et al. (2019) proposed a waste collection routing optimization model to minimize total energy consumption by converting the traditional waste collection into a cyber-physical system using Industry 4.0 technology and intelligent monitoring technology.

Geographic information system (GIS) is also applied to optimize garbage collection routing. Based upon the actual road conditions provided by GIS, such as road inclination, one-way roads, and narrow roads, Şebnem Düzgun et al. (2016) formulated a vehicle routing problem model to minimize the travel distance. According to the real situations in the developing countries, Vu et al. (2018) summarized the waste collection process into two stages: pre-collection and collection. During the pre-collection stage, the waste was collected by a cart or a small compactor and transported to a movable temporary collection point (TCP) for temporary storage. In the collection stage, a larger truck was used to transport

the waste from TCP to the waste disposal station. They applied GIS to monitor the capacity and distribution of TCP and distance of waste to TCP in both stages.

Electric waste contains not only high-value recyclable materials but hazardous materials as well. Therefore, timely and efficient recycling of electronic waste is essential (Ma et al., 2015; Park et al., 2018). There are currently two ways of recycling: stationary and mobile (Nowakowski, 2017). Stationary recycling is the normal garbage collection, while mobile recycling is recycling on the roadside or on-site according to the requirements of residents or companies. Nowakowski et al. (2017) and Nowakowski et al. (2018) studied on-demand mobile recycling. Residents or companies filled out the electric waste form online, and then the recycling company would arrange appropriate recycling time and optimize vehicle routes. They developed a recycling support system in which four optimization algorithms were embedded to reduce operating costs and to reduce vehicle emissions (Nowakowski et al., 2018). The authors further considered the satisfaction of residents in the system and established a multi-criteria optimization model using fuzzy logic to improve recycling efficiency (Nowakowski et al., 2017).

Unlike residential waste, industrial waste has a larger amount and is usually concentrated in location; therefore, large waste containers are needed for bulk waste collection. Based upon the customers' requirements, Wy et al. (2013) defined seven types of industrial waste collection service types, such as whether the customer needs empty containers and whether the customer needs to return empty containers. To save industrial waste collection time and cost, Hauge et al. (2014) studied the continuous service problem with one truck loading multiple waste containers and one container serving multiple customers in a queue without returning the depot every time. They combined the column generation algorithm with a tabu search heuristic algorithm to solve the problem.

3. Vessel Routing Model for Marine Debris

This section discusses the vessel routing optimization for marine debris collection considering dynamic velocity and direction. Vessels need to be rented from privates or corporates and might have different volume capacities, weight capacities, and tank capacities. The vessels are dispatched to collect offshore debris when weather condition permits. This study refers to the offshore waters within 150 nautical miles of the coastline. When the initial location of debris is input into GNOME software, the corresponding time window of debris trajectory will be determined. The debris will stay around this location within the time window. As long as the vessel can arrive at the location within this time window, it is guaranteed that the debris would be successfully collected. Otherwise, the debris will transport further, which will increase the overall debris collection cost. The vessel is able to dispatch at any port and return to any port after completing the cleanup task. Debris sinking into the bottom and eaten by marine animals are not considered in this study.

Let $V_1 = \{1, \cdots, m\}$ be the vertex set of m origin harbors, $V_2 = \{m+1, \cdots, m+n\}$ the vertex set of n debris areas in the predicted locations, and $V_3 = \{m+n+1, \cdots, 2m+n\}$ the vertex set of m destination harbors. The set V_1 is the same as V_3. We separate them into two sets in order to facilitate the model, i.e., $V = V_1 \cup V_2 \cup V_3$ to be the set of all vertex. Let $A_1 = \{(i,j) | i \in V_1, j \in V_2\}$ be the arc set from origin harbor to debris location, $A_2 = \{(i,j) | i,j \in V_2, i \neq j\}$ be the arc set from one debris location to another, and $A_3 = \{(i,j) | i \in V_2, j \in V_3\}$ be the arc set from debris location to destination harbor, i.e., $A = A_1 \cup A_2 \cup A_3$ to be the set of all arcs. Let P and D be the set of debris vessels and the set of debris types, respectively.

Each debris location $i \in V_2$ has a collection time t_i. For each destination harbor $d \in V_3$, t_d, f_d^b, and f_d^u denote berth time, berth cost, and unloading cost, respectively. There is a time window $[t_i^e, t_i^l]$ for each vertex $i \in V$. If $i \in V_1$, then

t_i^e denotes the earliest start time for the collection work, and t_i^l is the latest finish time which is the infinity at origin harbor; if $i \in V_2$ then $[t_i^e, t_i^l]$ is the collection interval at the debris location; and if $i \in V_3$, then t_i^e is set 0, and t_i^l is the latest finish time for the collection work. Let the longitude and latitude of every vertex $i \in V$ be dx_i and dy_i, respectively. The volume of debris type $k \in D$ at debris location $i \in V_2$ is assumed by q_{ik}^v. Besides, each arc $(i,j) \in A$ has two associated nonnegative attributes: a length $dist_{ij}$ and a direction of debris vessel relative to the ground δ_{ij}.

For each debris vessel $p \in P$, we have the following cost: hourly fuel cost during sailing f_p^s, hourly fuel cost during collection in the sea or berth at destination harbor f_p^c, hourly rent cost f_p^r, hourly insurance cost f_p^a and hourly labor cost f_p^l, respectively. The other parameters related to vessel $p \in P$ are maximum velocity $l_p^{\max}$, minimum velocity $l_p^{\min}$, hourly fuel consumption during sailing b_p^s, hourly fuel consumption during collection or berth b_p^c, volume capacity C_p^v, weight capacity C_p^w and fuel tank capacity C_p^f, respectively.

The corresponding decision variables are described below. The binary variables, x_{ijp}, is equal to 1 if debris vessel $p \in P$ traverses arc $(i,j) \in A$ and 0 otherwise. The other four continuous variables are defined as follows: ta_{ip} is the arrival time at debris location $i \in V$ of debris vessel $p \in P$; Q_{ip}^v and Q_{ip}^w denote the cumulative volume and cumulative weight at debris location $i \in V$ in debris vessel $p \in P$, respectively; and the velocity variable of vessel $p \in P$ for arc $(i,j) \in A$ is defined by the velocity relative to the ground l_{ijp}.

Sets

V_1	Set of origin harbors, $V_1 = \{1, \cdots, m\}$,
V_2	Set of debris areas in the predicted location, $V_2 = \{m+1, \cdots, m+n\}$,
V_3	Set of destination harbors, $V_3 = \{m+n+1, \cdots, 2m+n\}$,
V	Set of all vertex, $V = V_1 \cup V_2 \cup V_3$,
A_1	Set of arcs from origin harbor to debris location, $A_1 = \{(i,j) \mid i \in V_1, j \in V_2\}$
A_2	Set of arcs from one debris location to another, $A_2 = \{(i,j) \mid i,j \in V_2, i \neq j\}$
A_3	Set of arcs from debris to destination harbor, $A_3 = \{(i,j) \mid i \in V_2, j \in V_3\}$
A	Set of all arcs, $A = A_1 \cup A_2 \cup A_3$,
P	Set of debris vessels,
D	Set of debris types,

Parameters

t_i	Collection time of debris location $i \in V_2$,
t_d	Berth time of destination harbor $d \in V_3$,
f_d^b	Berth cost at destination harbor $d \in V_3$,
f_d^u	Unloading cost at destination harbor $d \in V_3$,
$[t_i^e, t_i^l]$	Time window of vertex $i \in V$,
ρ_k	Density of debris type $k \in D$,
f_p^s	Hourly fuel cost of debris vessel $p \in P$ during sailing,
f_p^c	Hourly fuel cost of debris vessel $p \in P$ during collection in the sea or berth at destination harbor,
f_p^r	Hourly rent cost of debris vessel $p \in P$,
f_p^a	Hourly insurance cost of debris vessel $p \in P$,
f_p^l	Hourly labor cost of debris vessel $p \in P$,
$l_p^{\max}$	Maximum velocity of debris vessel $p \in P$,
$l_p^{\min}$	Minimum velocity of debris vessel $p \in P$,

b_p^s	Hourly fuel consumption of debris vessel $p \in P$ during sailing,
b_p^c	Hourly fuel consumption of debris vessel $p \in P$ during collection or berth,
C_p^w	Weight capacity of debris vessel $p \in P$
C_p^v	Volume capacity of debris vessel $p \in P$,
C_p^f	Fuel tank capacity of debris vessel $p \in P$,
q_{ik}^v	Volume of debris type $k \in D$ at debris location $i \in V_2$,
dx_i	The longitude of vertex $i \in V$,
dy_i	The latitude of vertex $i \in V$,
$dist_{ij}$	Length of arc $(i,j) \in A$,
δ_{ij}	Direction of debris vessel relative to the ground for arc $(i,j) \in A$,

Decision Variables

x_{ijp}	1 if debris vessel $p \in P$ traverses arc $(i,j) \in A$; 0 otherwise,
ta_{ip}	Arrival time at debris location $i \in V$ of debris vessel $p \in P$,
Q_{ip}^v	Cumulative volume at debris location $i \in V$ in debris vessel $p \in P$,
Q_{ip}^w	Cumulative weight at debris location $i \in V$ in debris vessel $p \in P$,
l_{ijp}	Velocity of debris vessel $p \in P$ relative to the ground for arc $(i,j) \in A$,

Distance Computation:

Because the earth is an ellipsoid, in order to accurately calculate the distance $dist_{ij}$ between the two locations, (dx_i, dy_i) and (dx_j, dy_j), we use the Haversine formula[2] as Eq. (1).

$$dist_{ij} = 2R\arcsin\sqrt{\sin^2\left(\frac{dy_j - dy_i}{2}\right) + \cos dy_j \cos dy_i \sin^2\left(\frac{dx_j - dx_i}{2}\right)} \quad (1)$$

In Eq. (1), R is the equatorial radius and takes 6378.137 kms.

Vessel Direction relative to the Ground Computation:

The relative rectangular coordinate system is adopted to shift the origin to the current point *i*. The longitude and latitude coordinate (dx_i, dy_i) of the current point *i* is changed to (0, 0), and the longitude and latitude coordinate (dx_j, dy_j) of point *j*, minus the longitude and latitude coordinate of the point *i* is $(dx_j - dx_i, dy_j - dy_i)$. So, the direction relative to the ground from location *i* to *j* for any vessel, δ_{ij}, can be derived according to Eq. (2).

$$\delta_{ij} = \arctan\frac{dy_j - dy_i}{dx_j - dx_i} \quad (2)$$

Proposed Model:

The proposed model for marine debris vessel routing problem with time windows considering winds and ocean currents is below:

$$\min F = \sum_{(i,j)\in A}\sum_{p\in P} f_p^s b_p^s \frac{dist_{ij}}{l_{ijp}} x_{ijp} + \sum_{(i,j)\in A_2}\sum_{p\in P} f_p^c b_p^c t_i x_{ijp} + \sum_{(i,d)\in A_3}\sum_{p\in P} f_p^c b_p^c t_d x_{idp} \quad (3)$$

[2]Available from: https://en.wikipedia.org/wiki/Haversine_formula.

$$+\sum_{(i,d)\in A_3}\sum_{p\in P}\left(f_d^b+f_d^u\right)x_{idp}+\sum_{d\in V_3}\sum_{i\in V_1}\sum_{p\in P}\left(f_p^r+f_p^a+f_p^l\right)\left(ta_{dp}+t_d-ta_{ip}\right)$$

$$\sum_{i\in V_1}\sum_{j\in V_2}x_{ijp}\le 1 \qquad p\in P \qquad (4)$$

$$\sum_{j\in V_2\cup V_3}\sum_{p\in P}x_{ijp}=1 \qquad i\in V_2 \qquad (5)$$

$$\sum_{j\in V_2\cup V_3}x_{ijp}=\sum_{j\in V_1\cup V_2}x_{jip} \qquad i\in V_2\,,\ p\in P \qquad (6)$$

$$\sum_{i\in V_1}\sum_{j\in V_2}x_{ijp}=\sum_{i\in V_2}\sum_{j\in V_3}x_{ijp} \qquad p\in P \qquad (7)$$

$$Q_{ip}^v+\sum_{k\in D}q_{jk}^v\le Q_{jp}^v+C_p^v(1-x_{ijp}) \qquad (i,j)\in A, p\in P \qquad (8)$$

$$Q_{ip}^w+\sum_{k\in D}\rho_k q_{jk}^v\le Q_{jp}^w+C_p^w(1-x_{ijp}) \qquad (i,j)\in A, p\in P \qquad (9)$$

$$\sum_{k\in D}q_{ik}^v\le Q_{ip}^v\le C_p^v \qquad i\in V_2, p\in P \qquad (10)$$

$$\sum_{k\in D}\rho_k q_{ik}^v\le Q_{ip}^w\le C_p^w \qquad i\in V_2, p\in P \qquad (11)$$

$$Q_{ip}^v=0 \qquad i\in V_1, p\in P \qquad (12)$$

$$Q_{ip}^w=0 \qquad i\in V_1, p\in P \qquad (13)$$

$$b_p^s\left(\sum_{d\in V_3}ta_{dp}-\sum_{i\in V_1}ta_{ip}\right)+(b_p^c-b_p^s)\sum_{i\in V_2}\sum_{j\in V_2\cup V_3}t_i x_{ijp}+b_p^c\sum_{i\in V_2}\sum_{d\in V_3}t_d x_{idp}\le C_p^f \qquad p\in P \qquad (14)$$

$$l_p^{\min}\le l_{ijp}\le l_p^{\max} \qquad (i,j)\in A, p\in P \qquad (15)$$

$$ta_{ip}+\frac{dist_{ij}}{l_{ijp}}\le ta_{jp}+M_{ijp}\left(1-x_{ijp}\right) \qquad (i,j)\in A_1\,, p\in P \qquad (16)$$

$$ta_{ip}+t_i+\frac{dist_{ij}}{l_{ijp}}\le ta_{jp}+M_{ijp}\left(1-x_{ijp}\right) \qquad i\in V_2, (i,j)\in A_2\cup A_3, p\in P \qquad (17)$$

$$t_j^e\sum_{i\in V_1\cup V_2}x_{ijp}\le ta_{jp}\le t_j^l\sum_{i\in V_1\cup V_2}x_{ijp} \qquad j\in V_2, p\in P \qquad (18)$$

$$ta_{dp}\ge t_d^e\sum_{i\in V_2}x_{dip} \qquad d\in V_1, p\in P \qquad (19)$$

$$ta_{dp} \le t_d^l \sum_{i \in V_2} x_{idp} \qquad d \in V_3, p \in P \qquad (20)$$

$$x_{ijp} \in \{0,1\} \qquad (i,j) \in A,\ p \in P \qquad (21)$$

$$ta_{ip}, Q_{ip}^v, Q_{ip}^w, l_{ijp} \ge 0 \qquad i \in V, (i,j) \in A,\ p \in P \qquad (22)$$

The objective function (3) minimizes the total debris collection costs. More specifically, the first three terms in (3) represent the fuel costs during sailing, collection in the sea, and berth at destination harbor, respectively. The fourth term in (3) represents the cost of berth and unloading at the destination harbor. The last term in the objective function depicts the sum of rent cost, insurance cost, and labor cost for every vessel. Constraint (4) guarantees that each vessel is assigned to a routing. Constraint (5) ensures that each debris location must be collected by only one debris vessel. Constraint (6) sets inflow equals outflow at each debris location. Constraint (7) forces the inflow into the destination harbor equal to the outflow from the origin harbor. Constraints (8)-(14) characterize volume, weight, and fuel tank restriction, respectively. Constraints (8) and (9) are used to calculate the cumulative volume and weight of collected debris at every location for each vessel routing, respectively. Constraints (10) and (11) limit the cumulative volume and weight in each vessel. Constraints (12) and (13) initialize the cumulative volume and weight in each vessel at the origin harbor. Constraint (14) limits fuel tank capacity. Constraint (15) is the maximum and minimum velocity limit. Constraints (16) and (17) compute arrival time of vessel at origin harbor and at each debris location and destination harbor, where $M_{ijp} = t_i^l + t_i + \frac{dist_{ij}}{l_p^{\min}}$. Constraint (18) enforces a time window for each debris location. Constraints (19) and (20) are the time windows at the origin harbor and destination harbor, respectively. Finally, constraints (21) and (22) set binary and nonnegativity restrictions.

Linearization:

The proposed formulation is a mixed-integer nonlinear programming model because of the presence of $(\frac{1}{l_{ijp}})$ term in the objective function (3) and in constraint (17). These two items can be linearized by introducing some additional variables, as illustrated below.

Let $z_{ijp} = \frac{1}{l_{ijp}}$. Objective function (3) and constraints (15)-(17) are then converted into the following (constraints 23-26).

$$\begin{aligned} \min F = & \sum_{(i,j)\in A} \sum_{p\in P} f_p^s dist_{ij} z_{ijp} x_{ijp} + \sum_{(i,j)\in A_2} \sum_{p\in P} f_p^c t_i x_{ijp} + \sum_{(i,d)\in A_3} \sum_{p\in P} f_p^c t_d x_{idp} \\ & + \sum_{(i,d)\in A_3} \sum_{p\in P} \left(f_d^b + f_d^u\right) x_{idp} + \sum_{d\in V_3} \sum_{i\in V_1} \sum_{p\in P} \left(f_p^r + f_p^a + f_p^l\right)\left(ta_{dp} + t_d - ta_{ip}\right) \end{aligned} \qquad (23)$$

$$ta_{ip} + dist_{ij} z_{ijp} \le ta_{jp} + M_{ijp}\left(1 - x_{ijp}\right) \qquad (i,j) \in A_1, p \in P \qquad (24)$$

$$ta_{ip} + t_i + dist_{ij} z_{ijp} \le ta_{jp} + M_{ijp}\left(1 - x_{ijp}\right) \qquad i \in V_2, (i,j) \in A_2 \cup A_3, p \in P \qquad (25)$$

$$\frac{1}{l_p^{\max}} \le z_{ijp} \le \frac{1}{l_p^{\min}} \qquad (i,j) \in A,\ p \in P \qquad (26)$$

Let $y_{ijp} = z_{ijp} x_{ijp}$, and objective function (23) is converted to the following:

$$\min F = \sum_{(i,j)\in A}\sum_{p\in P} f_p^s dist_{ij} y_{ijp} + \sum_{(i,j)\in A_2}\sum_{p\in P} f_p^c t_i x_{ijp} + \sum_{(i,d)\in A_3}\sum_{p\in P} f_p^c t_d x_{idp} + \sum_{(i,d)\in A_3}\sum_{p\in P}\left(f_d^b + f_d^u\right)x_{idp} + \sum_{d\in V_3}\sum_{i\in V_1}\sum_{p\in P}\left(f_p^r + f_p^a + f_p^l\right)\left(ta_{dp} + t_d - ta_{ip}\right) \quad (27)$$

Additionally, some linearization constraints should be added, as shown below in constrains (28)-(30).

$$y_{ijp} \le \frac{1}{l_p^{\min}} x_{ijp} \qquad (i,j)\in A,\ p\in P \qquad (28)$$

$$y_{ijp} \le z_{ijp} \qquad (i,j)\in A,\ p\in P \qquad (29)$$

$$y_{ijp} \ge z_{ijp} - \frac{1}{l_p^{\min}}(1 - x_{ijp}) \qquad (i,j)\in A,\ p\in P \qquad (30)$$

With this, an equivalent MILP model is formulated as follows.

$$\min F = \sum_{(i,j)\in A}\sum_{p\in P} f_p^s dist_{ij} y_{ijp} + \sum_{i\in V_2}\sum_{j\in V_2}\sum_{p\in P} f_p^c t_i x_{ijp} + \sum_{i\in V_2}\sum_{d\in V_3}\sum_{p\in P} f_p^c t_d x_{idp} + \sum_{(i,d)\in A_3}\sum_{p\in P}\left(f_d^b + f_d^u\right)x_{idp} + \sum_{d\in V_3}\sum_{i\in V_1}\sum_{p\in P}\left(f_p^r + f_p^a + f_p^l\right)\left(ta_{dp} + t_d - ta_{ip}\right) \quad (27)$$

subject to constraints: (4)-(14), (18)-(22), (24)-(26), (28)-(30), and

$$y_{ijp}, z_{ijp} \ge 0 \qquad i\in V, (i,j)\in A,\ p\in P \qquad (31)$$

Direction and Velocity of Debris Vessels relative to the Sea Calculation:

Winds and ocean currents have critical impacts on vessel routing. Because of these impacts, the actual velocity and direction of a vessel routing in the sea are different from what is observed on the ground. We assume the velocities and directions of winds and ocean currents and the direction of a vessel relative to the ground (from location *i* to location *j*) are constants. The velocity and direction of a vessel relative to the sea can be computed by a one-to-one mapping. Similarly, given the velocity and direction of a vessel relative to the sea, the velocity of a vessel relative to the ground can also be mapped. Thus, the velocity and direction of the resultant force, according to the velocities and directions of winds and ocean currents, will be calculated first. Then, the one-to-one mapping relationship will be obtained by taking the actual velocity and direction of a vessel relative to the sea as a function of the velocity of a vessel relative to the ground, and the other decision variables in the proposed model will be calculated as well. Finally, the values of the actual velocity and direction of a vessel relative to the sea can be obtained from the proposed one-to-one mapping. We assume radian mode for all angles belonging to $[0,2\pi)$ and all velocities are scalars.

Proposition 1 Suppose velocity v_f and direction $\propto_f$ of the resultant force, vessel *p* traveled from location *i* to *j* with the direction relative to the ground δ_{ij} and the velocity relative to the ground l_{ijp}, then its velocity v_{ijp} and direction β_{ijp} relative to the sea could be determined by the following Eqs. (32) and (33), respectively.

$$v_{ijp} = \left(v_f^2 + l_{ijp}^2 - 2v_f l_{ijp}\cos\left(\propto_f - \delta_{ij}\right)\right)^{\frac{1}{2}} \quad (32)$$

$$\beta_{ijp} = \begin{cases} \propto_f + \arccos\dfrac{v_{ijp}^2 + v_f^2 - l_{ijp}^2}{2v_f v_{ijp}} - \pi, & \text{if } \left(0 \le \propto_f - \delta_{ij} \le \pi \text{ and } \propto_f \ge \pi\right) \text{ or} \\ & \left(0 \le \propto_f - \delta_{ij} \le \pi, \propto_f < \pi \text{ and } l_{ijp}^2 \ge v_f^2 + v_{ijp}^2 + 2v_f v_{ijp}\cos \propto_f\right) \\ \propto_f + \arccos\dfrac{v_{ijp}^2 + v_f^2 - l_{ijp}^2}{2v_f v_{ijp}} + \pi, & \text{if } \left(0 \le \propto_f - \delta_{ij} \le \pi, \propto_f < \pi \text{ and } l_{ijp}^2 < v_f^2 + v_{ijp}^2 + 2v_f v_{ijp}\cos \propto_f\right) \text{ or } \delta_{ij} - \propto_f \ge \pi \\ \propto_f - \arccos\dfrac{v_{ijp}^2 + v_f^2 - l_{ijp}^2}{2v_f v_{ijp}} - \pi, & \text{if } \propto_f - \delta_{ij} > \pi \text{ or } \left(0 < \delta_{ij} - \propto_f < \pi, \delta_{ij} \ge \pi \text{ and } l_{ijp}^2 \le v_f^2 + v_{ijp}^2 + 2v_f v_{ijp}\cos \propto_f\right) \\ \propto_f - \arccos\dfrac{v_{ijp}^2 + v_f^2 - l_{ijp}^2}{2v_f v_{ijp}} + \pi, & \text{if } \left(0 < \delta_{ij} - \propto_f < \pi \text{ and } \delta_{ij} < \pi\right) \text{ or} \\ & \left(0 < \delta_{ij} - \propto_f < \pi, \delta_{ij} \ge \pi \text{ and } l_{ijp}^2 > v_f^2 + v_{ijp}^2 + 2v_f v_{ijp}\cos \propto_f\right) \end{cases} \tag{33}$$

Proof. See **Appendix A** for details.

Proposition 2 Suppose winds velocity v_w, winds direction $\propto_w$, ocean currents velocity v_c, ocean currents direction $\propto_c$, and their impact factors, θ_c and θ_w, used to describe their respective influences, the velocity, and direction of resultant force f, v_f and $\propto_f$, can be calculated using Eqs. (34) and (35), respectively.

$$v_f = (\theta_c^2 v_c^2 + \theta_w^2 v_w^2 + 2\theta_c\theta_w v_c v_w \cos(\propto_w - \propto_c))^{\frac{1}{2}} \tag{34}$$

$$\propto_f = \begin{cases} \propto_c + \arcsin\dfrac{\theta_w v_w \sin(\propto_w - \propto_c)}{v_f}, & \text{if } \propto_c \le \propto_w \\ \propto_w + \arcsin\dfrac{\theta_c v_c \sin(\propto_c - \propto_w)}{v_f}, & \text{if } \propto_c > \propto_w \end{cases} \tag{35}$$

Proof. See **Appendix A** for details.

4. Solution Algorithms

4.1 Branch-and-Cut (B&C) Algorithm

B&C algorithm is one of the most commonly used techniques to solve MILP problems (Padberg & Rinaldi, 1991; Hoffman & Padberg, 1993; Cordeau, 2006; Alizadeh et al., 2019a). This technique integrates the cutting plane method within a Branch-and-Bound (B&B) algorithm. In this study, a number of problem-specific valid inequalities and variable fixing techniques are developed, which are added to the root node of the B&B algorithm. Further, problem-specific logical cuts are added to the child nodes if violated. The aim is to trim the search tree to minimize the solution time.

Variable Fixing and Valid Inequalities:

In order to accelerate the computational performance of the B&C algorithm, we develop a few variable fixing techniques and valid inequalities, shown in constraints (36) to (39).

- If vessel $p \in P$, starting its trip from initial node $i \in V_1 \cup V_2$ to a debris location $j \in V_2$, is not able to satisfy the corresponding time window restriction; we then fix the respective variables to zero.

$$x_{ijp} = 0 \quad \forall p \in P, i \in V_1 \cup V_2, j \in V_2 \mid \frac{dist_{ij}}{v_p^{max}} \ge t_j^l \tag{36}$$

- If vessel $p \in P$ is unable to collect the debris in location $j \in V_2$ due to capacity restriction,, we fix the respective variables to zero.

$$\sum_{i\in V_1\cup V_2} x_{ijp} = 0 \quad \forall p \in P, j \in V_2 \mid \sum_{k\in D} \rho_k q_{jk}^v \geq c_p^w \ , \sum_{k\in D} q_{jk}^v \geq c_p^v \tag{37}$$

Beyond these fixing variables, we develop a set of valid inequalities:

- The below inequality provides a valid lower bound to the arc usage. To be specific, below inequalities considering the total weight and volume of the debris along with the weight and volume capacity of vessels will ensure that the minimum number of arcs to collect debris from all locations are opened throughout the network.

$$\sum_{i\in V_1\cup V_2}\sum_{j\in V_2}\sum_{p\in P} x_{ijp} \geq \left\lceil \max\left(\frac{\sum_{j\in V_2}\sum_{k\in D} q_{jk}^v}{\sum_{p\in P} c_p^v}, \frac{\sum_{j\in V_2}\sum_{k\in D} \rho_k q_{jk}^v}{\sum_{p\in P} c_p^w}\right)\right\rceil \tag{38}$$

- The vessel $p \in P$ is able to use any arc $(i,j) \in A$ if the arc is accessible within the feasible time window, t_w. Here, the term t_w represents the length of the planning horizon.

$$\sum_{i\in V_1\cup V_2}\sum_{j\in V_2\cup V_3} \frac{x_{ijp} dist_{ij}}{v_p^{max}} \leq t_w \quad \forall p \in P \tag{39}$$

Logical cuts:

- Another set of valid inequalities are defined to relax the time window constraint. For any $p \in P$, if the obtained trip $\{i_1, i_2, i_3, \dots, i_k\}$ violates the time window of the visited debris locations, we add the following constraint:

$$x_{i_1 i_2 p} + x_{i_2 i_3 p} + x_{i_3 i_4 p} + \cdots + x_{i_{k-1} i_k p} \leq |K| - 2 \tag{40}$$

- Similarly, we can relax the volumetric capacity and weight capacity constraints, and separately check that for any vessel $p \in P$, whether the obtained trip $\{i_1, i_2, i_3, \dots, i_k\}$ violates the respective volumetric and weight capacity. If any trip violates the mentioned capacities, we add the following constraint for the violated trip:

$$x_{i_1 i_2 p} + x_{i_2 i_3 p} + x_{i_3 i_4 p} + \cdots + x_{i_{k-1} i_k p} \leq |K| - 2 \tag{41}$$

4.2 Two-Stage Heuristic Approach

Our initial computational tests expose the inability of the GUROBI and the B&C algorithm to solve the proposed model in large-scale settings. This is primarily because our problem is an extension of the traditional VRP, which is already known to be an NP-hard problem (Karamyar et al., 2018). However, due to the fact that the location of debris will be changed over time, there is an urgent need to solve large-scale instances in a reasonable time period. To alleviate such challenges, this study proposes a two-stage heuristic approach. The first-stage utilizes an adaptive large neighborhood search (ALNS) heuristic with the fixed velocity values. Later, in the second-stage, a velocity optimization algorithm is utilized to improve the solution for each visited route.

Below, we provide details of the two-stage heuristic approach. However, before delving into the details of the first-stage ALNS algorithm, an initial route generation mechanism that can be applied in the ALNS algorithm is discussed.

Initial Routes Generation Mechanism

In order to generate initial feasible routes for vessels, we utilize the nearest neighbor heuristic algorithm (Kizilates & Nuriyeva, 2013). The quality of the generated routes utilizing this algorithm is better than the random initial routes, and therefore the computational time of the ALNS algorithm can be reduced. The algorithm is operated by gradually adding arcs starting from one harbor to one debris location. The insertion of debris location $i \in V_2$ is determined based upon the

respective time window and the remaining volumetric and weight capacity of vessel $p \in P$ (i.e., $[t_i^e, t_i^l], C_p^v, C_p^w$) as well as the fuel tank capacity of debris vessels (C_p^f). The process will continue to construct initial feasible routes for all the remaining debris vessels.

To further illustrate the framework of the Initial Route Generation mechanism, we first introduce the set $candidate^{total}$ that represents all the unvisited debris locations in the network. Further, $candidate^p$ is introduced to represent the unvisited and unallocated debris locations to the vessel $p \in P$. Steps of the Initial Route Generation mechanism are as follows:

a) Initialize the route for vessel $p \in P$ and $candidate^p \coloneqq candidate^{total}$

b) Find the nearest debris location $j \in candidate^p$ to the harbors $i \in V_1$

c) Check the time window restriction for the selected pair (i, j) if violated, remove j from the $candidate^p$, go to step 2; otherwise, start the route for vessel p with the current pair (i, j).

d) Find the nearest unvisited location j' in $candidate^p$ and remove it from $candidate^p$

e) Check the time window, weight, volume, and fuel restrictions, including j' in the route of vessel p, if not violated, go to j' and remove it from $candidate^{total}$

f) Check if there is any unvisited location left in $candidate^p$? If yes, go to step 4; otherwise, go to step 1

Stage I. Adaptive Large Neighborhood Search (ALNS) Algorithm

The ALNS Algorithm has been initially proposed by Ropke and Pisinger (2006a). This algorithm belongs to the class of very large-scale neighborhood algorithms (Pisinger & Ropke, 2010) and can be considered as an extension of the large neighborhood search algorithm developed by Shaw (1997). The ALNS allows the possibility of implementing multiple destructions and insertion operators simultaneously to generate high-quality solutions.

In the ALNS algorithm, to develop high-quality routes for debris vessels, a set of insertion and destruction operators indicated by $\boldsymbol{A}$ and $\boldsymbol{B}$, respectively, are defined firstly. ALNS algorithm is an iterative process, and in each iteration, one of the candidate destruction operators, i.e., $OP_b \in \boldsymbol{B}$, and one of the candidate insertion operators, i.e., $OP_a \in \boldsymbol{A}$ will be selected to make new routes for vessels. It is worth mentioning that the performance of the ALNS algorithm highly depends on the selection of the insertion and destruction operators; hence, the choice of the different OP_a and OP_b is of high importance to the success of the ALNS algorithm. To efficiently select the operators, Ropke and Pisinger (2006a) proposed a Roulette Wheel selection Mechanism, where each operator OP_a/OP_b has a weight W_{OP_a}/W_{OP_b} and a score π_{OP_a}/π_{OP_b}, which is collected from the prior performance of the operator. The roulette wheel mechanism is the most common and widely used selection mechanism, which assigns a selection probability to each member of an operator. Having defined the weight of each operator, we can define the probability of selecting OP_a as $P_{OP_a} \coloneqq W_{OP_a} / \sum_{a \in A} W_{OP_a}$. Similarly, $P_{OP_b} \coloneqq W_{OP_b} / \sum_{b \in B} W_{OP_b}$. In the first iteration of the ALNS algorithm, it is assumed that the weights for destruction and insertion operators are equal, i.e., $W_{OP_a} = 1; \forall a \in \boldsymbol{A}$ and $W_{OP_b} = 1; \forall b \in \boldsymbol{B}$, and the score of all the operators is equal to zero, i.e., $\pi_{OP_a} = 0; \forall a \in \boldsymbol{A}$ and $\pi_{OP_b} = 0; \forall b \in \boldsymbol{B}$.

At i^{th} iteration of the ALNS algorithm, the weight of operators ($W_{OP_m} | m \in \{\boldsymbol{A}, \boldsymbol{B}\}$) is updated as follow: $W_{OP_m}^i = W_{OP}^{i-1}{}_m (1 - \eta) + \eta(\pi_{OP_m}/\theta_m)$, where η is a reaction factor generated from a uniform distribution, $\eta \in [0,1]$, to show a reaction to changes on the operator performance, and θ_m is the number of times the corresponding operator has been

selected. In each iteration, in addition to updating the weights of selected operators, the scores of selected operators are updated as follow: the score is increased by σ_1 when the implementation of the operator leads to a global optimal solution; otherwise, the score is increased by σ_2/σ_3 when the fitness value of the obtained solution is better/worse than the fitness value of the solution generated in the previous iteration. Furthermore, the relation between the different amount of increases in the score is $\sigma_1 \geq \sigma_2 \geq \sigma_3$. Finally, to terminate the ALNS algorithm, two criteria have been adopted (i) the maximum iteration limit and (ii) the maximum computational time limit.

ALNS Operators

In the ALNS algorithm, different types of insertion and destruction operators are utilized. We now briefly describe each of these operators. Basically, a destruction operator removes a visited debris location(s) from a route(s), while an insertion operator inserts an unvisited debris location(s) into a route(s). A removal list for visited debris locations, $H_{Removal}$, a return list for unvisited debris locations, H_{return}, are developed for destruction and insertion operators, respectively, where $H_{Removal} \cap H_{Return} = \phi$. Note that before implementing the ALNS algorithm, all the debris locations are inserted into the H_{return}, i.e., $H_{Removal} = \phi, H_{Return} = V_2$. In the following, five destruction and four insertion operators are discussed that can be used within the ALNS algorithm.

Destruction Operators:

***Random Removal (RR)*:** This operator simply chooses p visited debris locations randomly from H_{return} according to a discrete uniform distribution, $U[1, |(H_{return})^{pr}|]$, and inserts them into $H_{removal}$, and updates H_{return}. Here, $(H_{return})^{pr}$ is the set of visited debris locations in the previous iteration of the algorithm. It is worth mentioning that the value is chosen for p $(p < |V_2|)$ has an impact on the number of iteration of the ALNS algorithm. Further, the random selection of visited debris locations via this operator increases the diversification into the search mechanism.

***Worst Removal (WR)*:** This operator removes debris location with the highly-visited cost from H_{return}, and replace the unvisited debris locations in $H_{removal}$ with the low-visited cost. Having obtained the highly-visited cost locations, both H_{return} and $H_{removal}$ are updated. This operator calculates the visited cost for all the debris locations in the H_{return}, and select q visited debris locations according to a non-increasing order of visited costs, inserts them into $H_{removal}$, and updates H_{return}. The visited cost of each debris location is defined as the difference between the costs when the debris is inserted into a route (i.e., visited) and removed from that route (i.e., unvisited). The obtained visit cost for each debris location in a route is normalized by dividing it to the average visited cost of all other debris locations that could be visited on that route. The goal of this normalization is to avoid repeatedly removing the debris locations which are located far away from the remaining debris locations.

***Route Removal (RoR)*:** This operator randomly selects one of the generated routes in the previous iteration of the algorithm and removes all the debris locations visited on that route from H_{return}. Then, all the visited route on the selected route are inserted into the $H_{removal}$, and both H_{return} and $H_{removal}$ are updated.

***History-based Removal (HKR)*:** This operator is working the same as the neighbor graph removal operator introduced by Ropke and Pisinger (2006b). This operator memorizes the position-based value of each debris location $i \in V_2$, where this value is determined as the sum of the distance between the location $i \in V_2$ and its preceding and following debris locations, all visited on the same route. In other words, the position-based value of a debris location i, P_i, is calculated as follow: $p_i := d_{(i-1,j)} + d_{(i,i+1)}$, where $d_{(i,j)}$ indicates the distance between two consecutive visited debris locations i and j in a generated route with the algorithm. The best position value of each debris location i, P'_i in iteration, k is determined in such a way that this value to be the minimum value of all P_i values related to the previous iterations $(k' <$

k). Afterward, this operator selects a debris location i' with a maximum deviation from its best position value, i.e., $i' = argmax_{i \in H_{return}}(P_i - P'_i)$. Then, the chosen debris location is removed from H_{return} and inserted into $H_{removal}$. Finally, both H_{return} and $H_{removal}$ are updated.

***Neighborhood Removal (NR)*:** This operator selects a debris location with maximum distance deviation from the average distance of its corresponding route. We assume that in iteration k, we have developed a set of routes as R^k. Considering route $r \in R^k$, we assume that n_r number of the debris locations $i \in V_2$ have been visited on this route as follow: $r = \{i_1, i_2, \dots, i_{n_r}\}$. Then the average distance of route r can be computed as follow: $\overline{d_r} := (\sum_{(i_1,i_2) \in r | i_1 \neq i_2} d_{(i_1,i_2)})/(n_r - 1)$, where $d_{(i_1,i_2)}$ represents the distance between two consecutive debris locations visited on route r. Having defined the average distance of a route, we need to remove debris location j from this route and calculate the average distance of that route, which gives us $\bar{d}_{r\setminus\{j\}}, \forall r \in R$. Afterward, a debris location s with the maximum deviation between $\overline{d_r}$ and $\bar{d}_{r\setminus\{j\}}$, is chosen, inserted to $H_{removal}$ and removed from H_{return}. Finally, both H_{return} and $H_{removal}$ are updated.

Insertion Operators

***Greedy Insertion (GI)*:** This operator inserts all the debris locations in $H_{removal}$ into the best possible position of existing routes based upon its insertion cost. The insertion cost of a debris location in $H_{removal}$ is computed as follow: $argmin_{i \in H_{return}, (j,k) \in H_{return}}(p'_{jik})$ and $p'_{jik} = d_{(j,i)} + d_{(i,k)} - d_{(j,k)}$, where j and k are the consecutive debris locations on the same route before adding debris location $i \in H_{return}$ between them.

***Greedy Insertion with Noise (GIN)*:** This operator is similar to Greedy insertion; however, once we want to calculate the insertion cost of debris locations in $H_{removal}$, a degree of freedom as a noise term needs to be considered. The insertion cost based on this degree of freedom can be expressed as $p'_{jik} = d_{(j,i)} + d_{(i,k)} - d_{(j,k)} + \alpha\rho\delta$, where α is the maximum distance between the debris locations $i, j,$ and k; ρ is a noise parameter used for diversification, which is set to be 0.1 and δ is a random number obtained from $[-1,1]$.

***Regret Insertion (RI)*:** For each debris location i in $H_{removal}$, we define δf_i^j, where this parameter indicates the insertion cost of debris location i visited on the j^{th} the best route at its best position. The debris location i' is selected as $i' = argmax_{i \in H_{removal}}(\delta f_i^1 - \delta f_i^2)$, where δf_i^1 and δf_i^2 are the first and second-best insertion costs of disaster-affected node i visited on the first and second-best route, respectively, at their best positions. Then, both H_{return} and $H_{removal}$ are updated, and this operator stops whenever all debris locations in $H_{removal}$ are inserted into the routes, i.e., $H_{removal} = \phi$.

***Regret Insertion with Noise (RIN)*:** Like GIN, this operator can be considered as an extension of regret operator (RI), where the best and second-best insertion costs of debris locations in $H_{removal}$ are calculated by considering a degree of freedom as a noise term, which is described in the GIN operator.

After implementing any operator described above, the current routes might be updated as follow: when it is determined that a debris location i in $H_{removal}$ needs to be inserted to a route, the feasibility of developed route with respect to volumetric and weight capacity (C_p^v, C_p^w) of utilizing vessel p for that route should be surveyed. If debris vessel $p \in P$ due to the violation of the mentioned restrictions is not capable of visiting all debris locations on the developed route, the developed route is ignored. Below, **Algorithm 1** presents the general framework of the ALNS algorithm with the abovementioned operators involved.

Algorithm 1: General Framework of the ALNS Algorithm

Input: $max_{itr}, max_{CT}, W_{OP_m}, \pi_{OP_m}; \forall m \in \{a, b\}, a \in \mathbf{A}, b \in \mathbf{B}$

Output: Best developed routes (S^{best})

Initialize $\sigma_1, \sigma_2,$ and σ_3

$P_{o_a} := \frac{1}{|\mathbf{A}|}; \forall a \in \mathbf{A}$ & $P_{o_b} := \frac{1}{|\mathbf{B}|}; \forall b \in \mathbf{B}$

$\pi_{o_a} := 0; \forall a \in \mathbf{A}$ & $\pi_{o_b} := 0; \forall b \in \mathbf{B}$

$S^{IR} \leftarrow Route.Initialization()$

$S^{best} \leftarrow S^{IR}$

$S \leftarrow S^{IR}$

While $i < max_{itr}$ *or* $CPU < max_{CT}$ **do**

Select a destruction operator op_b and an insertion operator op_a according to Roulette-wheel mechanism

$S' \leftarrow destruction.Operator.Implemantation(S)$

$S' \leftarrow Insertion.Operator.Implemantation(S)$

Update the value of θ_{op_m}; $\forall m \in \{a, b\}, a \in \mathbf{A}, b \in \mathbf{B}$

If $\left(CF(S') < CF(S)\right)$ **then**

If $\left(CF(S') < CF(S^{best})\right)$ **then**

$S^{best} \leftarrow S'$

Increase the score of the selected destruction and insertion operators be σ_1

Else

Increase the score of the selected destruction and insertion operators by σ_2

End

Else

Increase the score of the selected destruction and insertion operators by σ_3

End

Update $W^i_{OP_m} := W^{i-1}_{OP_m}(1-\eta) + \eta(\pi_{OP_m}/\theta_m), \forall m \in \{a, b\}, a \in \mathbf{A}, b \in \mathbf{B}$

Update $P^i_{Op_a} := \frac{W^i_{OP_a}}{\sum_{a \in A} W^i_{OP_a}}, \forall a \in \mathbf{A}$ & $P^i_{Op_b} := \frac{W^i_{OP_b}}{\sum_{b \in B} W^i_{OP_b}}, \forall b \in \mathbf{B}$

$S \leftarrow S'$

$i \leftarrow i + 1$

End

Return S^{best}

Stage II. Velocity Optimization:

Solving the debris vessel routing problem via the ALNS heuristic, a set of feasible routes, in terms of volumetric and weight capacity (C^v_p, C^w_p), will be found. The pseudo-code of the ALNS algorithm is provided in **Algorithm 1**. Assume that a feasible path $(0, \dots, n+1)$ is one of the obtained routes, which is served by one of the debris vessels $p \in P$. In this path, 0 and $n+1$ denote the port where the debris vessel $p \in P$ starts/ends its trip. In the following mathematical model, we will use the same notations as to the first proposed model. We also introduce an additional decision variable w_i to

represents the waiting time at each node $i \in (0, \dots, n+1)$.The formulation of the Velocity Optimization Problem (**VOP**) for vessel $p \in P$ is as follows:

$$Min\ F' = ta_{n+1,p} - ta_{0p} \quad (42)$$

$$ta_{i+1,p} = ta_{ip} + w_i + t_i + \frac{dist_{i,i+1}}{l_{i,i+1,p}} \qquad i = 0, \dots, n \quad (43)$$

$$t_i^e \le ta_{ip} + w_i \le t_i{}^l \qquad i = 0, \dots, n \quad (44)$$

$$t_i^e \le ta_{ip} + w_i \le t_i{}^l \qquad i = 0, \dots, n+1 \quad (45)$$

$$l_p^{\min} \le l_{i,i+1,p} \le l_p^{\max} \qquad i = 0, \dots, n \quad (46)$$

$$w_i, l_{i,i+1,p} \ge 0 \qquad i = 0, \dots, n \quad (47)$$

$$ta_{ip} \ge 0 \qquad i = 0, \dots, n+1 \quad (48)$$

The objective function (42) minimizes the total travel time associated with each debris vessel $p \in P$. As a result, the cost related to the fuel consumption along with the insurance, labor, and rent cost of the debris vessel $p \in P$ is minimized accordingly. Constraint (43) ensures that the arrival time of debris vessel $p \in P$ in node $i \in (0, \dots, n+1)$ is equal to the sum of the arrival time at node i, waiting time at node i, debris collecting time at node i, and sailing time to i. Constraint (44) and (45) guarantee the fact that the debris collection in $i \in (0, \dots, n+1)$ should be started in the respective time window. Constraint (46) is to ensure that the velocity of the debris vessel does not violate the respective velocity limit. Constraints (47) and (48) impose non-negativity restrictions on the variables.

As we can see, constraint (43) is nonlinear due to the presence of the $(\frac{dist_{i,i+1}}{l_{i,i+1,p}})$ term. Here we introduce a new variable $Z_{i,i+1,p} = \frac{1}{l_{i,i+1,p}}$ to linearize the model. By doing so, a linearized model is obtained, which is described below:

$$Min\ F' = ta_{n+1,p} - ta_{0p} \quad (49)$$

$$ta_{i+1,p} = ta_{ip} + w_{ip} + t_i + dist_{i,i+1} Z_{i,i+1,p} \qquad i = 0, \dots, n \quad (50)$$

$$t_i^e \le ta_{ip} + w_{ip} \le t_i{}^l \qquad i = 0, \dots, n \quad (51)$$

$$t_i^e \le ta_{ip} + w_{ip} \le t_i{}^l \qquad i = 0, \dots, n+1 \quad (52)$$

$$\frac{1}{l_p^{\min}} \leq Z_{i,i+1,p} \leq \frac{1}{l_p^{\max}} \qquad i = 0, \dots, n \quad (53)$$

$$w_{ip}, Z_{i,i+1,p} \geq 0 \qquad i = 0, \dots, n \quad (54)$$

$$ta_{ip} \geq 0 \qquad i = 0, \dots, n+1 \quad (55)$$

For a given route of vessel $p \in P$ which is obtained from the first stage of the ALNS heuristic, the **VOP** model is applied. If the solution space of this model is feasible, then the debris vessel velocity and arrival time in its respective route is revised. Otherwise, if the solution space of the **VOP** is infeasible, then the obtained route violates the time window restrictions and should be ignored. After all, using the optimized arrival time, the fuel usage of the debris vessel (p) with respect to its fuel capacity (C_p^f) is surveyed. If the mentioned restrictions are violated, the developed route is not capable of visiting all debris locations on the developed route, and as such, should be ignored as well.

5. Computational Study and Managerial Insights

This section presents the computational results in solving the proposed mathematical model using the B&C and Two-stage heuristic approach and draws a number of managerial insights by developing a real-life case study. The proposed mathematical model and the solution algorithms are coded in Python 2.7 on a desktop with Intel Core i7 3.6 GHz processor and 32.0 GB RAM. GUROBI Optimizer 6.5[3] is used to solve the optimization model and solution approaches. Although the case study locations might not be within the marine debris rich area, it is sufficient to validate the proposed model and solution approach.

All the data used in this study is extracted directly from Duan et al. (2020). **Table B1 & 2** in **Appendix B** summarizes the key input parameters used in the optimization model. **Figure 3** shows the initial distribution of debris to our test regions. We consider three different harbors: Boston, Gloucester, and Situate at the State of Massachusetts, U.S., as the testing ground to visualize and validate the modeling results. All costs are calculated based on the 2019 U.S. dollar value.

The first set of experiments study the impact of dynamic debris dispersion on the debris collection. Marine debris locations continuously change over time. To better examine this impact, we investigate the movement of the 30 initial debris locations over a week, which is illustrated in **Figure 4**. **Figure 4a** is showing the initial location of debris, while **Figures 4b** to **d** represent the location of debris after two, four, and six days of the initial day, respectively. As we can see, the location of debris on the third day is getting closer to the harbors; however, in the following days, they start to get far away from the harbors. This is caused by the combined force of the local wind, ocean current, tidal, and other geological impacts. To demonstrate the impact on the debris collection performance, we use these four positions as four different cases, as defined below:

- **Case 1**: Initial location (Day 1; 8:00 am) (**Figure 4a**)
- **Case 2**: location (Day 3; 8:00 am) (**Figure 4b**)
- **Case 3**: location (Day 5; 8:00 am) (**Figure 4c**)

[3]Available from: http://www.gurobi.com/

- **Case 4**: location (Day 7; 8:00 am) (**Figure 4d**)

Figure 3 Initial distribution of debris

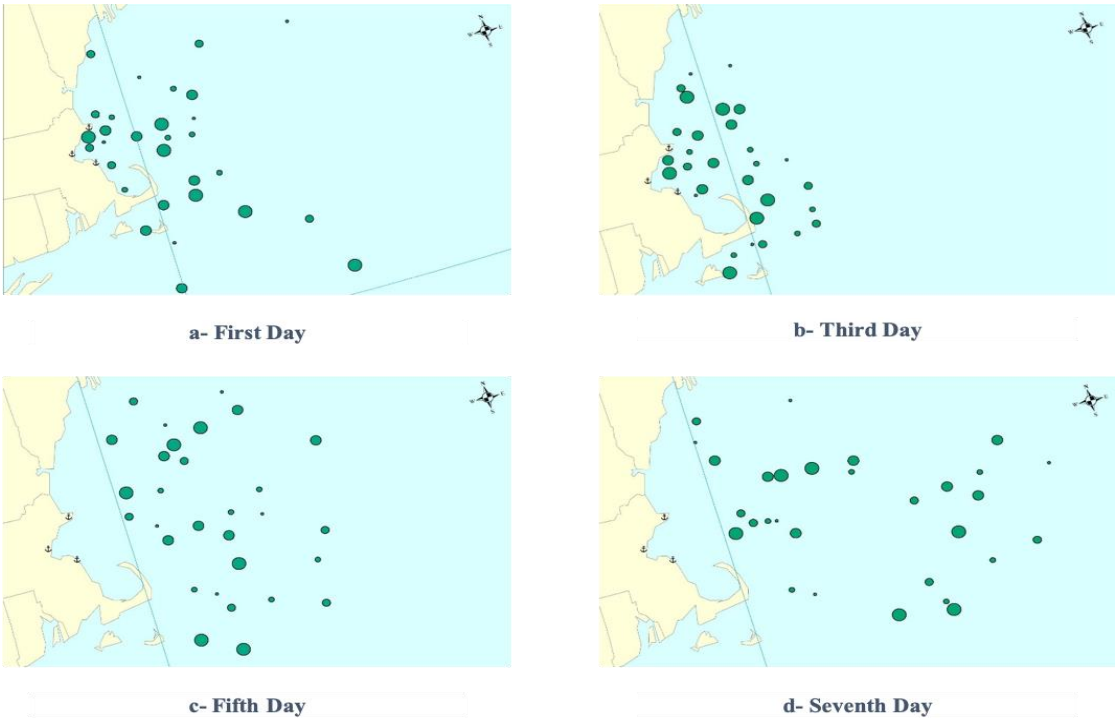

Figure 4 Debris dispersion representation on the first, third, fifth, and seventh days

The experimental results from these four generated cases are presented in **Figure 5**. The key findings are summarized as below:

- If debris is collected from the initial locations (Case 1), the daily collection cost is approximately $6,142. In Case 2, debris locations are getting closer to harbors, and the overall collecting cost drops by 18% from the initial case. However, in Case 3 and Case 4, the location of debris starts to get far away from harbors, and as a result, the overall collecting cost increases by 5% and 17%, respectively, from Case 1.
- In Case 1, on average, 70% of the capacity of debris vessels is used to collect the marine debris. When debris is closer to harbors (Case 2), fewer vessels are required to collect the debris, and the average usage of capacity of

vessels increases to 91%. However, in Case 3 and 4, as the debris gets further away from the harbors, the vessel's average capacity is utilized by 76% and 57%, respectively.

- It can be realized that Case 2 shows the best result in terms of debris collection cost and the more efficient capacity usage of vessels. In Case 2, due to the ocean-related factors such as tidal issues and direction of the wind, the GNOME Software predicts that the debris locations would be nearer to the harbors compared to other days. Therefore, capturing the ocean-related factors and predicting locations of marine debris based on these factors for a set of days in a week, the best day to dispatch vessels to collect the debris can be determined accordingly.
- **Figure 5b** also points out that when the debris is more dispersed (Case 4), vessels need to use, on average, 0.45 gallons of fuel to collect each cubic foot of debris. This amount can be reduced to 0.12 gallons when the debris comes closer to the shore (Case 2).

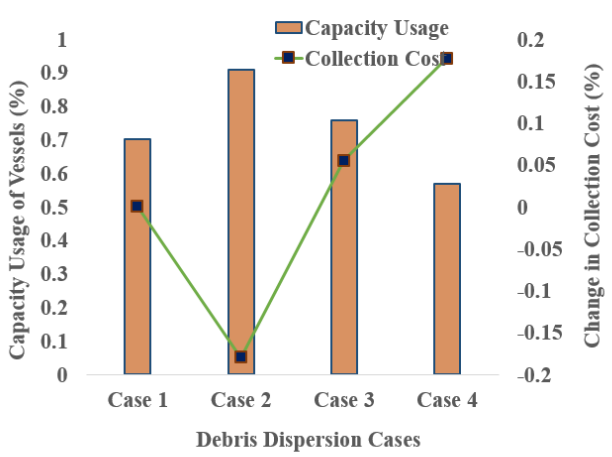

a-Impact of debris dispersion in overall debris collection cost and average usage of vessels capacity

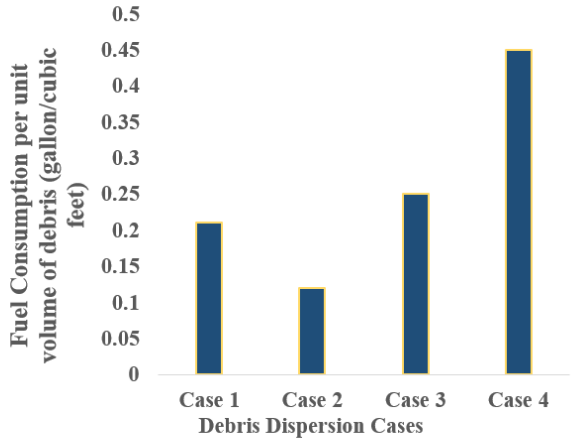

b-Impact of debris dispersion in fuel consumption

Figure 5 Impact of debris dispersion of vessel capacity utilization and fuel consumption

The second set of experiments investigates the impact of debris collection distance on the overall collection cost and volume. Marine debris is generally widely spread in the ocean. Due to the limitation of a vessel on the range and capacity, it is expensive to deploy vessels in the longer distances. To better investigate this impact, we split our selected debris collection area into five ranges, as shown in **Figure 6**. These ranges are defined as follows:

- **Range 1**: Collection range is within 50 miles from the selected harbors
- **Range 2**: Collection range is within 80 miles from the selected harbors
- **Range 3**: Collection range is within 110 miles from the selected harbors
- **Range 4**: Collection range is within 140 miles from the selected harbors
- **Range 5**: Any range greater than 140 miles

Note that Range 3 points to the initial debris location and is the same to our selected case (Case 1) discussed previously. The results are summarized in **Figures 7-9**. The main findings are summarized below:

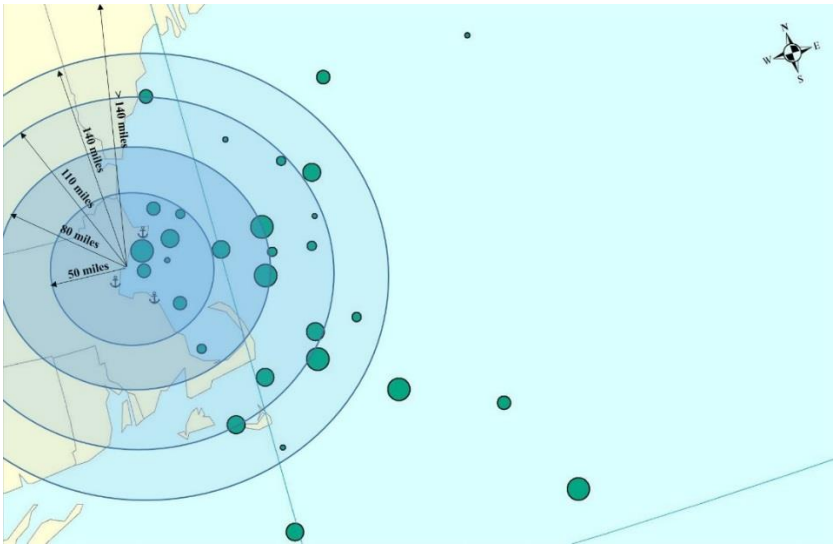

Figure 6 Debris location (in day 1) and different ranges

- As the debris collection range decreases, the overall collecting cost also decreases. **Figure 7** demonstrates that when the selected range is Range 5, all the 30 debris locations have been taken into account, and the overall collecting cost is $5,788. However, when Range 4 is selected, the overall collecting cost is decreased to $2,785. Similarly, for the following ranges (3, 2, and 1), it can be seen that the overall collecting cost compared to the immediate prior range is decreased by $153, $1,374, and $581, respectively. As can be seen, the difference in collecting cost between two successive collecting ranges is not changing monotonically, and the maximum difference is between Range 4 and 5 ($2,785). Hence, it can be realized that considering all 30 debris locations (Range 5) to collect the debris is not an efficient decision for the current experiments.

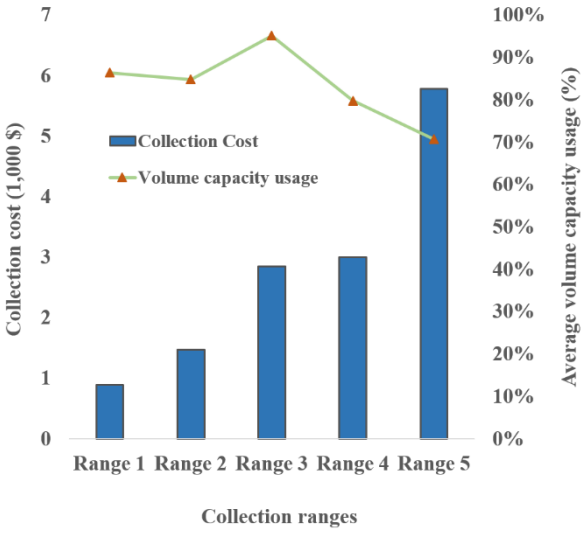

Figure 7 Impact of debris collection distance in overall debris collection cost and vessel usage

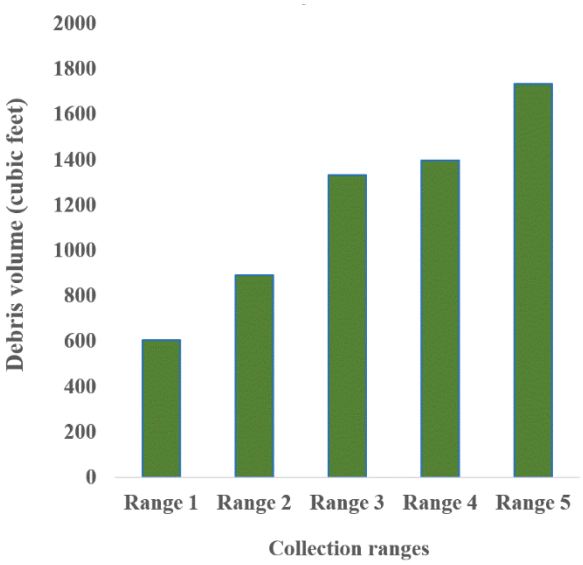

Figure 8 Debris collection volume

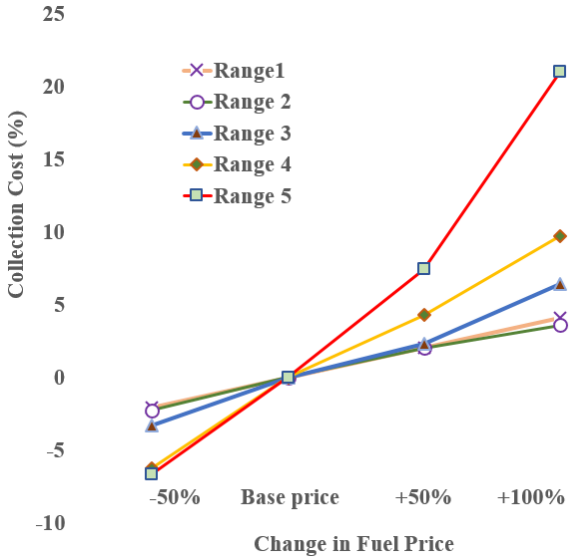

Figure 9 Collection cost sensitivity to fuel price

- **Figure 7** demonstrates that the best usage of the capacity of vessels is Range 3 (approximately 95%). When we choose to collect the debris in Ranges 2 and 4, on average, approximately 11% and 16% less capacity of vessels will be utilized over Range 3.
- As the collection radius is increased, a larger volume of debris can be collected subsequently. For instance, when the collection range increases from 2 to 3, the amount of debris collection is increased by around 49% (see **Figure 8**). It can be seen that the maximum percentage of change in collected debris volume is from Range 2 to 3.
- From **Figures 7** and **8**, we can conclude that given the five test ranges and the application areas on hand, Range 3 (within 110 miles from the harbor) will be more effective. This means that any distance beyond this range will extensively increase the overall debris collection cost.
- **Figure 9** conducts sensitivity analysis by varying the fuel price by -50%, +50%, +100%, and +150% on the five ranges defined earlier. Notice that by restricting the debris collection within 110 miles (Ranges 1, 2, and 3), the overall collection cost varies from -3.2% to +6.4%. However, the collection cost becomes highly sensitive (-6.5% to +21.2%) in fuel price when we chose Range 4 for debris collection.

We now experiment with the computation performance of B&C and two-stage heuristic approaches in solving the proposed mathematical model. To do so, we vary set $|V_2|, |D|$, and $|P|$ to generate six different problem instances. The descriptions of these instances are summarized in **Table 1**. **Table 2** summarizes the computational performance of the solution approaches in solving the marine debris model using the problem instances described in **Table 1**. The $\epsilon(\%)$ in **Table 2** represents the optimality gap obtained by the respective solution approaches. Note that the two-stage heuristic only provides a valid upper bound (UB_{TS}) for the original problem. Therefore, we use the lower bound obtained from the B&C algorithm ($LB_{B\&C}$) to approximate the optimality gap for the two-stage heuristic, namely, $\epsilon(\%) = \left(\frac{UB_{TS} - \mathrm{LB}_{\mathrm{B\&C}}}{UB_{TS}}\right) \times 100$. Hence, the actual gap for the two-stage heuristic might be less than the reported gap. Further, we set a 10.0% optimality gap for the GUROBI and B&C algorithm and a 5.0% optimality gap for the two-stage heuristic. Additionally, a

time limit of 32,400 seconds is set for GUROBI, B&C, and the two-stage heuristic. Finally, the boldface letters under *t*(sec) column in **Table 2** indicates the best computational time (in seconds) between the proposed solution approaches and GUROBI.

Table 1 Problem instances with sizes

Instance	Case	($\|V_1\|=\|V_3\|$)	$\|V_2\|$	$\|D\|$	$\|P\|$	Variable			Total constraints
						Binary	Continuous	Total Variables	
Small	1	3	10	3	3	450	996	1,446	5,155
	2	3	10	5	5	750	1,660	2,410	6,585
Medium	3	3	20	3	6	3,000	6,312	9,312	33,310
	4	3	20	5	9	4,500	9,468	13,968	39,955
Large	5	3	30	3	10	10,500	21,720	32,220	108,180
	6	3	30	5	13	13,650	28,236	41,886	121,725

Table 2 Performance comparison among B&C, Two-stage heuristic, and GUROBI solver

Case	GUROBI		B&C		Two-stage heuristic	
	$\epsilon(\%)$	$t(sec)$	$\epsilon(\%)$	$t(sec)$	$\epsilon(\%)$	$t(sec)$
1	9.79	16,293	9.93	9,007	3.36	**264**
2	9.62	18,803	9.47	10,996	2.84	**427**
3	9.91	31,082	9.61	15,193	2.91	**795**
4	15.11	32,400	9.87	19,514	3.12	**1,134**
5	24.83	32,400	9.97	28,021	3.61	**1,689**
6	35.95	32,400	14.27	32,400	4.83	**2,289**
Average	17.53	27,230	10.52	19,189	3.44	**1,099**

Results indicate that GUROBI is only able to solve the first 3 problem instances, B&C can solve 5 cases and two-stage heuristic is able to solve all cases. The quality of the solution obtained by different algorithms directly depends on the quality of the corresponding optimality gaps. Hence, the lower optimality gap provides better solutions for the problem. The results in **Table 2** indicate that, on average, the GUROBI and B&C algorithm provides 17.53% and 10.52% optimality gaps, respectively, by obeying the prespecified termination criteria. On the other hand, the two-stage heuristic provides roughly 17 and 24 times faster solution over the B&C algorithm and GUROBI, respectively, while maintaining a competitive optimality gap of 3.44%. Overall, the two-stage heuristic seems to provide high-quality solutions consistently.

6. Conclusion

As more research has been conducted to reveal the harms of marine debris, how to effectively mitigate the risk has become essential. In this paper, we applied the logistics network method to collect offshore floating macro-marine debris in order to minimize the total cost. We formulated this problem as a generalized vessel routing problem with time windows (VRPTWs) consideration, involving vessel velocity relative to the ground as an additional decision variable. To the best of our knowledge, this is the first study to consider the impacts of ocean currents and winds on both debris trajectory and the direction and velocity of the vessel. After vessel routing and velocity relative to the ground being optimized, the actual velocity and direction relative to the sea can be computed according to the one-to-one mapping between velocity and direction relative to the ground and the sea under the influence of winds and ocean currents. In addition, for different

scaleproblems, two algorithms are proposed, namely, the Branch-and-Cut (B&C) algorithm and the Adaptive Large Neighborhood Search (ALNS) algorithm. The results show that the proposed ALNS algorithm can generate consistent, high-quality solutions for the large-scale problems in a reasonable time. Finally, a case study in the vicinity of Boston is used to validate the modeling results and to reveal a number of managerial insights, such as the impacts of dynamic debris dispersion and debris collection distances on the overall system performance.

The major contributions of this paper are as follows: (i) introducing a realistic vessel routing problem for debris collection, where the debris locations and vessel velocity and direction are influenced by winds and ocean currents; (ii) employing GNOME software to predict and track the debris trajectory and proposing a mapping mechanism to describe the relationship between velocity and direction relative to the ground and the sea, given winds and ocean currents; (iii) designing and testing B&C algorithm and ALNS algorithm to solve large scale problem instances; and (iv) distilling managerial insights from a case study for marine debris collection.

Although this study has many merits, it still has several drawbacks that need to be further investigated. First, further study is needed to improve the prediction accuracy of debris trajectory. The exact location of debris has a crucial impact on the collection process. This is because, for every 0.1-degree difference in longitude or latitude, the distance varies by about 10 km. Two approaches can be undertaken: (i) using a more accurate predictive method or software, or (ii) adopting a stochastic programming modeling approach. Second, integrate the debris disposal process on the land with the collection process in the ocean to optimize the whole debris handling process. These issues will be studied in the future studies.

Appendix A

In this section, we prove **Proposition 1** and **Proposition 2**. Obviously, when vessel p is not assigned to j from i, i.e., $x_{ijp} = 0$, the corresponding velocity v_{ijp} and direction β_{ijp} relative to the sea must be 0. In other words, v_{ijp} and β_{ijp} can only be greater than 0 when $x_{ijp} = 1$. Next, we will prove that the two equations hold when $x_{ijp} = 1$. Note that even if $x_{ijp} = 1$, β_{ijp} may still be equal to 0. And all the following angles are calculated counterclockwise from the starting line to the ending line.

Proposition 1 Given velocity v_f and direction $\propto_f$ of the resultant force, vessel p traveled from location i to j with the direction relative to the ground δ_{ij} and the velocity relative to the ground l_{ijp}, then its velocity v_{ijp} and direction β_{ijp} relative to the sea could be determined by the following (32) and (33), respectively.

$$v_{ijp} = \left(v_f^2 + l_{ijp}^2 - 2v_f l_{ijp} \cos\left(\propto_f - \delta_{ij}\right)\right)^{\frac{1}{2}} \tag{32}$$

$$\beta_{ijp} = \begin{cases} \propto_f + \arccos\dfrac{v_{ijp}^2 + v_f^2 - l_{ijp}^2}{2v_f v_{ijp}} - \pi, & \text{if } \left(0 \le \propto_f - \delta_{ij} \le \pi \text{ and } \propto_f \ge \pi\right) \text{ or} \\ & \quad \left(0 \le \propto_f - \delta_{ij} \le \pi, \propto_f < \pi \text{ and } l_{ijp}^2 \ge v_f^2 + v_{ijp}^2 + 2v_f v_{ijp}\cos \propto_f\right) \\ \propto_f + \arccos\dfrac{v_{ijp}^2 + v_f^2 - l_{ijp}^2}{2v_f v_{ijp}} + \pi, & \text{if } \left(0 \le \propto_f - \delta_{ij} \le \pi, \propto_f < \pi \text{ and } l_{ijp}^2 < v_f^2 + v_{ijp}^2 + 2v_f v_{ijp}\cos \propto_f\right) \text{ or } \delta_{ij} - \propto_f \ge \pi \\ \propto_f - \arccos\dfrac{v_{ijp}^2 + v_f^2 - l_{ijp}^2}{2v_f v_{ijp}} - \pi, & \text{if } \propto_f - \delta_{ij} > \pi \text{ or } \left(0 < \delta_{ij} - \propto_f < \pi, \delta_{ij} \ge \pi \text{ and } l_{ijp}^2 \le v_f^2 + v_{ijp}^2 + 2v_f v_{ijp}\cos \propto_f\right) \\ \propto_f - \arccos\dfrac{v_{ijp}^2 + v_f^2 - l_{ijp}^2}{2v_f v_{ijp}} + \pi, & \text{if } \left(0 < \delta_{ij} - \propto_f < \pi \text{ and } \delta_{ij} < \pi\right) \text{ or} \\ & \quad \left(0 < \delta_{ij} - \propto_f < \pi, \delta_{ij} \ge \pi \text{ and } l_{ijp}^2 > v_f^2 + v_{ijp}^2 + 2v_f v_{ijp}\cos \propto_f\right) \end{cases}$$

(33)

Proof. There are a total of eight cases to be considered.

Case 1 $0 \leq \propto_f - \delta_{ij} \leq \pi$ and $\propto_f \geq \pi$.

Since $0 \leq \propto_f - \delta_{ij} \leq \pi$ and $\propto_f \geq \pi$, no matter what values of $\propto_f$ and δ_{ij} take, in order to form a parallelogram with the velocity and direction of a vessel relative to the ground as a diagonal; there must be $0 \leq \beta_{ijp} \leq \delta_{ij}$ and $0 \leq \propto_f - \beta_{ijp} \leq \pi$, as shown in **Figure A.1**. The quadrilateral $iAjB$ is a parallelogram. Vector iA, ij, and iB denote the resultant force, velocity, and direction relative to the ground and velocity and direction relative to the sea, respectively. The dotted line iC is parallel to the horizontal axis. So, we have $|iA| = |Bj| = v_f, |ij| = l_{ijp}, |iB| = |Aj| = v_{ijp}$, and $\angle CiA = \propto_f, \angle Cij = \delta_{ij}, \angle CiB = \beta_{ijp}$. In triangle iAj, $\angle jiA = \propto_f - \delta_{ij}$, according to the law of cosines, there must be $|Aj|^2 = |iA|^2 + |ij|^2 - 2|iA||ij|\cos\angle jiA$, i.e., $v_{ijp} = \left(v_f^2 + l_{ijp}^2 - 2v_f l_{ijp}\cos\left(\propto_f - \delta_{ij}\right)\right)^{\frac{1}{2}}$. (32) holds in **Case 1**.

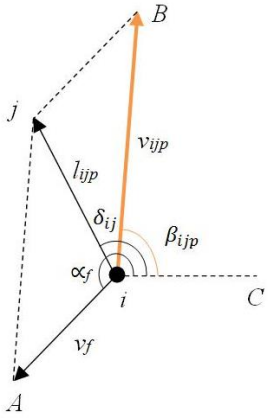

Figure A.1 $0 \leq \propto_f - \delta_{ij} \leq \pi$ and $\propto_f \geq \pi$ in **Case 1**

In parallelogram $iAjB$, $\angle iAj = \pi - \angle BiA = \pi - (\angle CiA - \angle CiB) = \pi - (\propto_f - \beta_{ijp})$. In triangle iAj, according to the law of cosines, there must be $|ij|^2 = |Aj|^2 + |iA|^2 - 2|Aj||iA|\cos\angle iAj$, i.e., $l_{ijp}^2 = v_f^2 + v_{ijp}^2 - 2v_f v_{ijp}\cos\left(\pi - (\propto_f - \beta_{ijp})\right)$. We have that

$$\beta_{ijp} = \propto_f + \arccos\frac{v_{ijp}^2 + v_f^2 - l_{ijp}^2}{2v_f v_{ijp}} - \pi.$$

So, (33) holds in **Case 1**.

Case 2 $0 \leq \propto_f - \delta_{ij} \leq \pi$ and $\propto_f < \pi$.

When $0 \leq \propto_f - \delta_{ij} \leq \pi$ and $\propto_f < \pi$, in order to form a parallelogram with the velocity of a vessel relative to the ground as a diagonal, there are two possibilities for the value range of β_{ijp}: **Case 2.1** $\beta_{ijp} \leq \delta_{ij}$; and **Case 2.2** $\beta_{ijp} > \pi$. They are shown in **Figures A.2** and **A.3**, respectively. The symbols for these lines and angles in both figures are the same as those in **Figure A.1**. We can not determine the value range of β_{ijp} until it's calculated. However, its value range is related to the difference between l_{ijp}^2 and $v_f^2 + v_{ijp}^2 + 2v_f v_{ijp}\cos \propto_f$. We will prove this equivalence next.

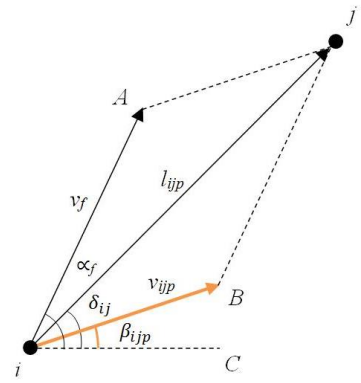

Figure A.2 $\beta_{ijp} \leq \delta_{ij}$ in **Case 2.1**

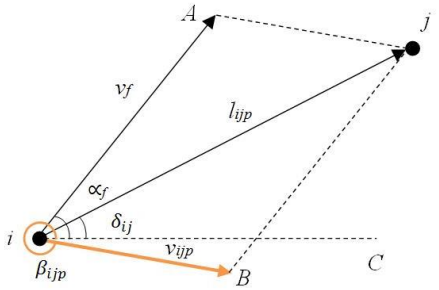

Figure A.3 $\beta_{ijp} > \pi$ in **Case 2.2**

In either case, there is $\angle jiA = \propto_f - \delta_{ij}$. So, (32) holds according to the law of cosines in triangle iAj.

After calculating v_{ijp} by (32), let $\beta_{ijp} = 0$ first. We construct a new parallelogram with v_f and v_{ijp} as two adjacent edge lengths, as shown in **Figure A.4**. In the parallelogram $iAkD$ in **Figure A.4**, $|iA| = v_f, \angle DiA = \propto_f, |iD| = v_{ijp}$, and the edge iD is parallel to the horizontal axis, that is, $\beta_{ijp} = 0$. The edge ik is the diagonal of the parallelogram $iAkD$, and $|ik| = r_{ijp}$. In triangle iDk, it holds that $r_{ijp}^2 = v_f^2 + v_{ijp}^2 - 2v_f v_{ijp}\cos(\pi - \propto_f)$.

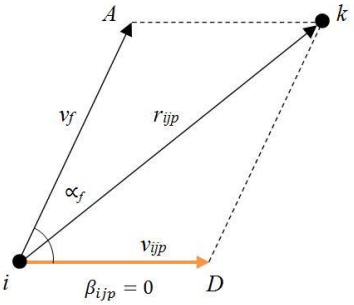

Figure A.4 A new parallelogram under $\beta_{ijp} = 0$ in **Case 2**

When $\beta_{ijp} \leq \delta_{ij}$ shown as in **Figure A.2**, the (A.1) holds in triangle iAj.

$$l_{ijp}^2 = v_f^2 + v_{ijp}^2 - 2v_f v_{ijp}\cos\left(\pi - (\propto_f - \beta_{ijp})\right) \tag{A.1}$$

When $\beta_{ijp} > \pi$, shown as in **Figure A.3**, (A.2) holds in triangle iAj.

$$l_{ijp}^2 = v_f^2 + v_{ijp}^2 - 2v_f v_{ijp}\cos\left(\pi - (2\pi - (\beta_{ijp} - \propto_f))\right) = v_f^2 + v_{ijp}^2 - 2v_f v_{ijp}\cos(\beta_{ijp} - \propto_f - \pi) \tag{A.2}$$

On the one hand, when $l_{ijp}^2 \geq r_{ijp}^2$, we have $-\cos(\pi - (\propto_f - \beta_{ijp})) \geq -\cos(\pi - \propto_f)$ or $-\cos(\beta_{ijp} - \propto_f - \pi) \geq -\cos(\pi - \propto_f)$. Since $\pi - (\propto_f - \beta_{ijp}), \beta_{ijp} - \propto_f - \pi$, and $\pi - \propto_f$ belong to an interval $(0, \pi)$, and cosine decreases in this interval, $\pi - (\propto_f - \beta_{ijp}) \geq \pi - \propto_f$ or $\beta_{ijp} - \propto_f - \pi \geq \pi - \propto_f$ holds. The results show that $\beta_{ijp} \geq 0$ or $\beta_{ijp} \geq 2\pi$. Obviously, only $\beta_{ijp} \geq 0$ can be taken. Further, if $\pi - (\propto_f - \beta_{ijp}) \leq \pi$, there must be $\beta_{ijp} \leq \propto_f$. In order to form a parallelogram with ij as its diagonal, there must be $\beta_{ijp} \leq \delta_{ij}$. When $l_{ijp}^2 \geq r_{ijp}^2$, $\beta_{ijp} \leq \delta_{ij}$ must hold. On the other hand, if $0 \leq \beta_{ijp} \leq \delta_{ij} \leq \propto_f$, then $\pi - \propto_f \leq \pi - (\propto_f - \beta_{ijp}) \leq \pi$. This leads to $l_{ijp}^2 \geq r_{ijp}^2$. Notice that $r_{ijp}^2 = v_f^2 + v_{ijp}^2 + 2v_f v_{ijp}\cos \propto_f$. Therefore, $l_{ijp}^2 \geq v_f^2 + v_{ijp}^2 + 2v_f v_{ijp}\cos \propto_f$ is equivalent to $\beta_{ijp} \leq \delta_{ij}$.

Similar to the above certification process, on the one hand, when $l_{ijp}^2 < r_{ijp}^2$, we have $\beta_{ijp} < 0$ or $\beta_{ijp} < 2\pi$. Obviously, only $\beta_{ijp} < 2\pi$ can be taken. And if $\beta_{ijp} - \propto_f - \pi > 0$, there must be $\beta_{ijp} > \pi$. When $l_{ijp}^2 < r_{ijp}^2$, $\beta_{ijp} > \pi$ must hold. On the other hand, if $\pi < \beta_{ijp} < 2\pi$, then $0 < \beta_{ijp} - \propto_f - \pi < \pi - \propto_f$. This leads to $l_{ijp}^2 < r_{ijp}^2$. Therefore, $l_{ijp}^2 < v_f^2 + v_{ijp}^2 + 2v_f v_{ijp}\cos \propto_f$ is equivalent to $\beta_{ijp} > \pi$.

Case 2.1 $l_{ijp}^2 \geq v_f^2 + v_{ijp}^2 + 2v_f v_{ijp}\cos \propto_f$.

According to the equivalence of $\beta_{ijp} \leq \delta_{ij}$ and $l_{ijp}^2 \geq v_f^2 + v_{ijp}^2 + 2v_f v_{ijp}\cos \propto_f$ and (A.1), it holds that

$$\beta_{ijp} = \propto_f + \arccos\frac{v_{ijp}^2 + v_f^2 - l_{ijp}^2}{2v_f v_{ijp}} - \pi.$$

The first equation in (33) holds in **Case 2.1**.

Case 2.2 $l_{ijp}^2 < v_f^2 + v_{ijp}^2 + 2v_f v_{ijp}\cos \propto_f$.

According to the equivalence of $\beta_{ijp} > \pi$ and $l_{ijp}^2 < v_f^2 + v_{ijp}^2 + 2v_f v_{ijp}\cos \propto_f$ and (A.2), it holds that

$$\beta_{ijp} = \propto_f + \arccos\frac{v_{ijp}^2 + v_f^2 - l_{ijp}^2}{2v_f v_{ijp}} + \pi.$$

The second equation in (33) holds in **Case 2.2**.

Case 3 $\delta_{ij} - \propto_f \geq \pi$.

Since $\delta_{ij} - \propto_f \geq \pi$, in order to form a parallelogram with the velocity and direction of a vessel relative to the ground as a diagonal, there must be $\propto_f \leq \beta_{ijp} \leq \delta_{ij}$ and $\beta_{ijp} - \propto_f \geq \pi$, as shown in **Figure A.5**. In triangle iAj, $\angle Aij = \left(2\pi - \left(\delta_{ij} - \propto_f\right)\right)$, according to the law of cosines, (32) holds in **Case 3**.

In parallelogram $iAjB$, $\angle iAj = \pi - \angle BiA = \pi - \left(2\pi - (\angle CiB - \angle CiA)\right) = \beta_{ijp} - \propto_f - \pi$. In triangle iAj, according to the law of cosines, there must be $l_{ijp}^2 = v_f^2 + v_{ijp}^2 - 2v_f v_{ijp}\cos\left(\beta_{ijp} - \propto_f - \pi\right)$, i.e.,

$$\beta_{ijp} = \propto_f + \arccos\frac{v_{ijp}^2 + v_f^2 - l_{ijp}^2}{2v_f v_{ijp}} + \pi.$$

So, the second equation in (33) holds in **Case 3**.

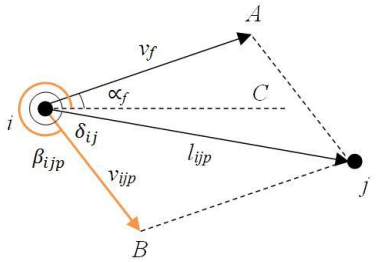

Figure A.5 $\delta_{ij} - \propto_f \geq \pi$ in **Case 3**

Case 4 $\propto_f - \delta_{ij} > \pi$.

Since $\propto_f - \delta_{ij} > \pi$, there must be $\beta_{ijp} > \delta_{ij}$ and $\propto_f - \beta_{ijp} > \pi$, as shown in **Figure A.6**. In triangle iAj, owing to $\angle Aij = \left(2\pi - \left(\propto_f - \delta_{ij}\right)\right)$, according to the law of cosines, (32) holds in **Case 4**.

In parallelogram $iAjB$, $\angle jAi = \pi - \angle AiB = \propto_f - \beta_{ijp} - \pi$. In triangle iAj, according to the law of cosines, there must be $l_{ijp}^2 = v_f^2 + v_{ijp}^2 - 2v_f v_{ijp}\cos\left(\propto_f - \beta_{ijp} - \pi\right)$, i.e.,

$$\beta_{ijp} = \propto_f - \arccos\frac{v_{ijp}^2 + v_f^2 - l_{ijp}^2}{2v_f v_{ijp}} - \pi.$$

So, the third equation in (33) holds in **Case 4**.

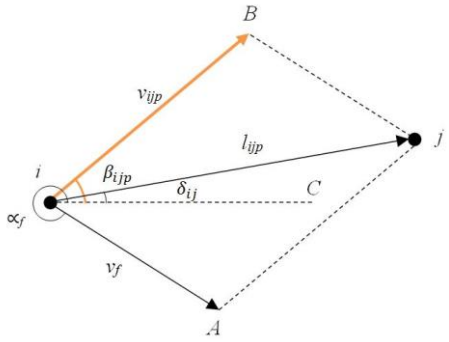

Figure A.6 $\propto_f - \delta_{ij} > \pi$ in **Case 4**

Case 5 $0 < \delta_{ij} - \propto_f < \pi$ and $\delta_{ij} \geq \pi$.

Similar to **Case 2**, when $0 < \delta_{ij} - \propto_f < \pi$ and $\delta_{ij} \geq \pi$, there are also two possibilities for the value range of β_{ijp}: **Case 5.1** $\beta_{ijp} > \delta_{ij}$; and **Case 5.2** $\beta_{ijp} < \propto_f$, shown as **Figures A.7** and **A.8**, respectively. And they are equivalent to $l_{ijp}^2 > v_f^2 + v_{ijp}^2 + 2v_f v_{ijp}\cos \propto_f$ and $l_{ijp}^2 \leq v_f^2 + v_{ijp}^2 + 2v_f v_{ijp}\cos \propto_f$.

In either cases, there is $\angle Aij = \delta_{ij} - \propto_f$. So, (32) holds according to the law of cosines in triangle iAj.

We also construct a new parallelogram with v_f and v_{ijp} calculated by (32) as two adjacent edge lengths, as shown in **Figure A.9**. In the parallelogram $iAkD$ in **Figure A.9**, $|iA| = v_f, \angle DiA = \propto_f, |iD| = v_{ijp}$, and the edge iD is parallel to the horizontal axis, that is, $\beta_{ijp} = 0$. The edge ik is the diagonal of the parallelogram $iAkD$, and $|ik| = r_{ijp}$. In triangle iDk, it holds that $r_{ijp}^2 = v_f^2 + v_{ijp}^2 - 2v_f v_{ijp}\cos(\propto_f - \pi) = v_f^2 + v_{ijp}^2 + 2v_f v_{ijp}\cos \propto_f$.

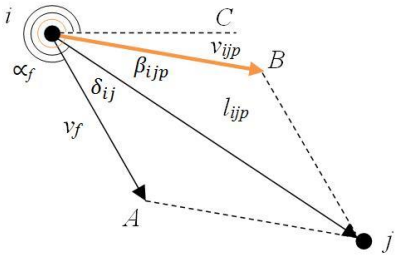

Figure A.7 $\beta_{ijp} > \delta_{ij}$ in **Case 5.1**

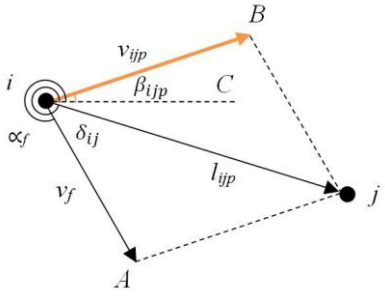

Figure A.8 $\beta_{ijp} < \propto_f$ in **Case 5.2**

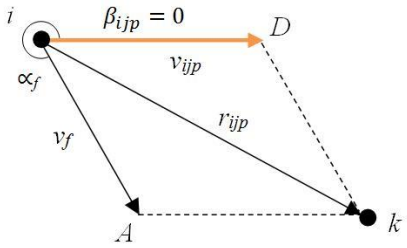

Figure A.9 A new parallelogram under $\beta_{ijp} = 0$ in **Case 5**

When $\beta_{ijp} > \delta_{ij}$, shown as in **Figure A.7**, the (A.3) holds in triangle iAj.

$$l_{ijp}^2 = v_f^2 + v_{ijp}^2 - 2v_f v_{ijp}\cos\left(\pi - (\beta_{ijp} - \propto_f)\right) \tag{A.3}$$

When $\beta_{ijp} < \propto_f$, shown as in **Figure A.8**, the (A.4) holds in triangle iAj.

$$l_{ijp}^2 = v_f^2 + v_{ijp}^2 - 2v_f v_{ijp}\cos\left(\pi - (2\pi - (\beta_{ijp} - \propto_f))\right) = v_f^2 + v_{ijp}^2 - 2v_f v_{ijp}\cos(\propto_f - \beta_{ijp} - \pi) \tag{A.4}$$

On the one hand, when $l_{ijp}^2 > r_{ijp}^2$, we have $\pi - (\beta_{ijp} - \propto_f) > \propto_f - \pi$ or $\propto_f - \beta_{ijp} - \pi > \propto_f - \pi$. Obviously, the result is $\beta_{ijp} < 2\pi$, which means $\beta_{ijp} > \delta_{ij}$ (**Case 5.1**), and $\beta_{ijp} < 0$ is abandoned. On the other hand, if $\beta_{ijp} > \delta_{ij}$, since $\beta_{ijp} < 2\pi$, we have $\pi - \beta_{ijp} > -\pi$. It means that $\pi - \beta_{ijp} + \propto_f > \propto_f - \pi$, i.e., $l_{ijp}^2 > r_{ijp}^2$. Therefore, $l_{ijp}^2 > v_f^2 + v_{ijp}^2 + 2v_f v_{ijp}\cos \propto_f$ is equivalent to $\beta_{ijp} > \delta_{ij}$.

Similar to the above certification process, on the one hand, when $l_{ijp}^2 \le r_{ijp}^2$, we have $\beta_{ijp} \ge 0$ which means $\beta_{ijp} < \propto_f$ (**Case 5.2**) and $\beta_{ijp} \ge 2\pi$ is abandoned. Further, if $\beta_{ijp} < \propto_f$, then $\propto_f - \beta_{ijp} - \pi \le \propto_f - \pi$ since $\beta_{ijp} \ge 0$. It leads to $l_{ijp}^2 \le r_{ijp}^2$. Therefore, $l_{ijp}^2 \le v_f^2 + v_{ijp}^2 + 2v_f v_{ijp}\cos \propto_f$ is equivalent to $\beta_{ijp} < \propto_f$.

Case 5.1 $l_{ijp}^2 > v_f^2 + v_{ijp}^2 + 2v_f v_{ijp}\cos \propto_f$.

According to the equivalence of $\beta_{ijp} > \delta_{ij}$ and $l_{ijp}^2 > v_f^2 + v_{ijp}^2 + 2v_f v_{ijp}\cos \propto_f$ and (A.3), it holds that

$$\beta_{ijp} = \propto_f - \arccos\frac{v_{ijp}^2 + v_f^2 - l_{ijp}^2}{2v_f v_{ijp}} + \pi.$$

The fourth equation in (33) holds in **Case 5.1**.

Case 5.2 $l_{ijp}^2 \le v_f^2 + v_{ijp}^2 + 2v_f v_{ijp}\cos \propto_f$.

According to the equivalence of $\beta_{ijp} < \propto_f$ and $l_{ijp}^2 \le v_f^2 + v_{ijp}^2 + 2v_f v_{ijp}\cos \propto_f$ and (A.4), it holds that

$$\beta_{ijp} = \propto_f - \arccos\frac{v_{ijp}^2 + v_f^2 - l_{ijp}^2}{2v_f v_{ijp}} - \pi.$$

The third equation in (33) holds in **Case 5.2**.

Case 6 $0 < \delta_{ij} - \propto_f < \pi$ and $\delta_{ij} < \pi$.

Similar to **Case 4**, since $0 < \delta_{ij} - \propto_f < \pi$ and $\delta_{ij} < \pi$, there must be $\beta_{ijp} > \delta_{ij}$ and $\beta_{ijp} - \propto_f < \pi$, as shown in **Figure A.10**. In triangle iAj, owing to $\angle Aij = \delta_{ij} - \propto_f$, according to the law of cosines, (32) holds in **Case 6**.

In parallelogram $iAjB$, $\angle jAi = \pi - \angle AiB = \pi - (\beta_{ijp} - \propto_f)$. In triangle iAj, according to the law of cosines, there must be $l_{ijp}^2 = v_f^2 + v_{ijp}^2 - 2v_f v_{ijp}\cos\left(\pi - (\beta_{ijp} - \propto_f)\right)$, i.e.,

$$\beta_{ijp} = \propto_f - \arccos\frac{v_{ijp}^2 + v_f^2 - l_{ijp}^2}{2v_f v_{ijp}} + \pi.$$

So, the fourth equation in (33) holds in **Case 6**.

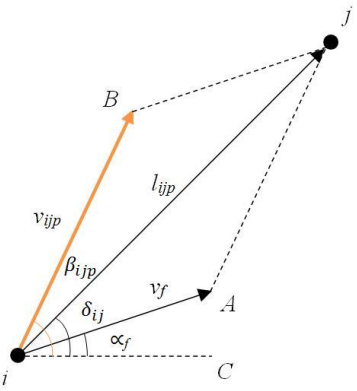

Figure A.10 $0 < \delta_{ij} - \propto_f < \pi$ and $\delta_{ij} < \pi$ in **Case 6**

To sum up, in all cases, we can get the (32) and (33). ■

The velocity and direction of resultant force *f* are computed by the following **Proposition 2**.

Proposition 2 Given winds velocity v_w, winds direction $\propto_w$, ocean currents velocity v_c, ocean currents direction $\propto_c$, and their factors θ_c and θ_w, the velocity and direction of resultant force *f*, v_f and $\propto_f$, can be calculated by (34) and (35), respectively.

$$v_f = (\theta_c^2 v_c^2 + \theta_w^2 v_w^2 + 2\theta_c\theta_w v_c v_w \cos(\propto_w - \propto_c))^{\frac{1}{2}} \tag{34}$$

$$\propto_f = \begin{cases} \propto_c + \arcsin\frac{\theta_w v_w \sin(\propto_w - \propto_c)}{v_f}, & \text{if } \propto_c \leq \propto_w \\ \propto_w + \arcsin\frac{\theta_c v_c \sin(\propto_c - \propto_w)}{v_f}, & \text{if } \propto_c > \propto_w \end{cases} \tag{35}$$

Proof. According to the magnitude relationship between $\propto_c$ and $\propto_w$, there are two cases to be considered.

Case 1 $\propto_c \leq \propto_w$

Case 1.1 $0 \leq \propto_w - \propto_c < \pi$.

There are many possibilities for the values of the resultant force and winds and ocean currents under **Case 1**, one of which is shown as **Figure A.11**. No matter in which case, there must be $\propto_c \leq \propto_f \leq \propto_w$.

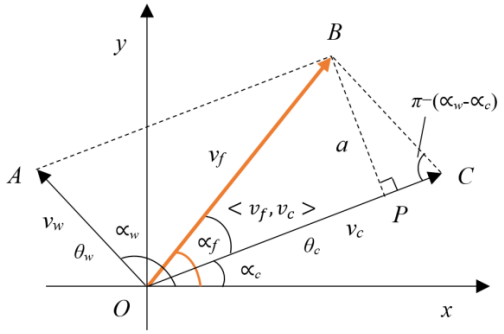

Figure A.11 $0 \leq \propto_w - \propto_c < \pi$ in **Case 1**

Because of angle $\angle COA = \propto_w - \propto_c$, angle $\angle BCO = \pi - (\propto_w - \propto_c)$. According to the law of cosines, in triangle *OCB*,

v_f can be obtained as follows.

$$v_f = (\theta_c^2 v_c^2 + \theta_w^2 v_w^2 - 2\theta_c\theta_w v_c v_w \cos(\pi - (\propto_w - \propto_c))^{\frac{1}{2}} = (\theta_c^2 v_c^2 + \theta_w^2 v_w^2 + 2\theta_c\theta_w v_c v_w \cos(\propto_w - \propto_c))^{\frac{1}{2}}.$$

Line segment *BP* is perpendicular to line segment *OC* at point *P* in triangle *OBC*, and *a* is the length of the segment *BP*. In the right triangle *BPC*,

$$a = \theta_w v_w \sin(\pi - (\propto_w - \propto_c)) = \theta_w v_w \sin(\propto_w - \propto_c).$$

Let $< v_c, v_f >$ be the angle formed by rotating counterclockwise from ocean currents vector $\vec{c}$ to the resultant force vector $\vec{f}$. In rectangular triangle *OPB*, we have

$$sin < v_c, v_f >= \frac{a}{v_f},$$

that is,

$$< v_c, v_f >= \arcsin \frac{\theta_w v_w \sin(\propto_w - \propto_c)}{v_f}.$$

Therefore,

$$\propto_f = \propto_c + < v_c, v_f >= \propto_c + arcsin \frac{\theta_w v_w sin(\propto_w - \propto_c)}{v_f}.$$

Case1.2 $\propto_w - \propto_c \geq \pi$.

There are two cases, $\propto_f > \propto_w$ and $\propto_f < \propto_c$, in **Case 1.2,** as shown in **Figures A.12** and **A.13,** respectively. No matter in which case, the results are the same. We will prove the former case.

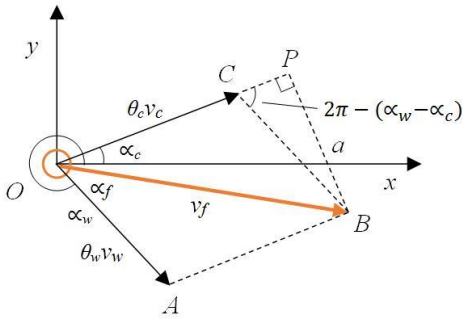

Figure A.12 $\propto_f > \propto_w$ in **Case 1.2**

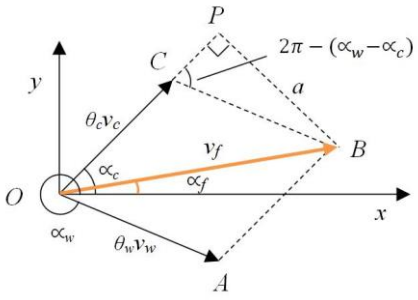

Figure A.13 $\propto_f < \propto_c$ in **Case 1.2**

Because of $\propto_w - \propto_c \geq \pi$, there must be $\angle AOC = \angle BCP = 2\pi - (\propto_w - \propto_c)$ and angle $\angle$ OCB $= \propto_w - \propto_c - \pi$. According to the law of cosines, in triangle OCB, v_f can be obtained as follows.

$$v_f = (\theta_c^2 v_c^2 + \theta_w^2 v_w^2 - 2\theta_c\theta_w v_c v_w \cos(\propto_w - \propto_c - \pi))^{\frac{1}{2}}$$

$$= (\theta_c^2 v_c^2 + \theta_w^2 v_w^2 + 2\theta_c\theta_w v_c v_w \cos(\propto_w - \propto_c))^{\frac{1}{2}}.$$

Line segment *BP* is perpendicular to line segment *OC* at point *P* in triangle *OCB*, and *a* is the length of the segment *BP*.

$$a = \theta_w v_w \sin(2\pi - (\propto_w - \propto_c)) = -\theta_w v_w \sin(\propto_w - \propto_c).$$

In rectangular triangle *OPB*, we have

$$\sin(2\pi - < v_c, v_f >) = -\sin(< v_c, v_f >) = \frac{-a}{v_f} = \frac{\theta_w v_w \sin(\propto_w - \propto_c)}{v_f},$$

that is,

$$< v_c, v_f >= \arcsin \frac{\theta_w v_w \sin(\propto_w - \propto_c)}{v_f}.$$

Therefore,

$$\propto_f = \propto_c + < v_c, v_f >= \propto_c + \arcsin \frac{\theta_w v_w \sin(\propto_w - \propto_c)}{v_f}.$$

Because of the symmetry of winds and ocean currents in Eqs. (1) and (2) in the content, the result of **Case 2** will be changed from **Case 1** by exchanging the subscripts *c* and *w* of corresponding parameters as follows.

$$v_f = (\theta_c^2 v_c^2 + \theta_w^2 v_w^2 + 2\theta_c \theta_w v_c v_w cos(\propto_c - \propto_w))^{\frac{1}{2}},$$

$$< v_f, v_w >= \arcsin \frac{\theta_C v_C sin(\propto_c - \propto_w)}{v_f},$$

$$\propto_f = \propto_w + < v_f, v_w >,$$

where $< v_f, v_w >$ be the angle formed by rotating counterclockwise from winds vector $\vec{w}$ to resultant force vector $\vec{f}$.

Case 2 $\propto_c > \propto_w$.

Similar to **Case 1**, there are two cases: $0 < \propto_c - \propto_w < \pi$ and $\propto_c - \propto_w \geq \pi$. The only difference is to exchange the position of $\propto_c$ and $\propto_w$. So, the result of $\propto_f$ in **Case 2** is also to exchange the position of $\propto_c$ and $\propto_w$ of it in **Case 1**. And the result of v_f is the same as it in **Case 1**.

To sum up, in all cases, we can get (34) and (35).

Appendix B

Tables B1 and **B2** present some of the important input parameters for the model and case study. **Table B1** shows three types of vessels and relevant information, and **Table B2** presents marine debris and harbor relevant information.

Table B1 Vessel Input Parameters

Parameter	Type A Vessel	Type B Vessel	Type C Vessel
Weight Capacity	6 tons	7 tons	8.5 tons
Volumn Capacity	353 ft^3	353 ft^3	353 ft^3
Fuel Tank Capacity	50 gallons	70 gallons	100 gallons
Max Velocity	10 knot	12 knot	12 knot
Min Velocity	6.7 knot	8 knot	8 knot

Rent Cost	\$250/day	\$300/day	\$350/day
Insurance Cost	\$2.74.day		
Berth Cost	\$90.2/berth		
Labor Cost	\$18~23/hr		

Table B2 Marine Debris and Harbor Input Parameters

Parameter	**Value**
Fuel Cost	gasoline \$2.98/gallon, diesel \$2/gallon
Carbon Emission Factor	Gasoline 10,180g; diesel 11,200g
Carbon Capacity	2800 tons per year
Berth Time of Destination Harbor	1~2 hr
Unloading Cost in Destination Harbor	\$40~50/unloading
Hourly Fuel Consumption at Max Velocity	8~10 gallons
Time Window of Debris Area	0.5~8 hr
Collection Time of Debris Area	0.5~2 hr
Density of Debris	0.6~1 g/cm^3

References

Angelini, Z., Kinner, N., Thibault, J., Ramsey, P., Fuld, K., 2019. Marine debris visual identification assessment. Marine Pollution Bulletin 142, 69-75.

Alizadeh, M., Ma, J., Mahdavi-Amiri, N., Marufuzzaman, M., Jaradat, R., 2019a. A stochastic programming model for a capacitated location-allocation problem with heterogeneous demands. Computers & Industrial Engineering 137, 106055.

Alizadeh, M., Ma, J., Marufuzzaman, M., Yu, F., 2019b. Sustainable olefin supply chain network design under seasonal feedstock supplies and uncertain carbon tax rate. Journal of Cleaner Production 222, 280-299.

Ballance, A., Ryan, P.G., Turpie, J.K., 2000. How much is a clean beach worth? The impact of litter on beach users in the Cape Peninsula. South Africa. South African Journal of Science 96, 210-213.

Bányai, T., Tamás, P., Illés, B., Stankevičiūtė, Ž., Bányai, Á., 2019. Optimization of municipal waste collection routing: impact of industry 4.0 technologies on environmental awareness and sustainability. International Journal of Environmental Research and Public Health 16, 634.

Barnes, D.K., Galgani, F., Thompson, R.C., Barlaz, M., 2009. Accumulation and fragmentation of plastic debris in global environments. Philosophical Transactions of the Royal Society B 364, 1985-1998.

Bauer-Civiello, A., Loder, J., Hamann, M., 2018. Using citizen science data to assess the difference in marine debris loads on reefs in Queensland, Australia. Marine Pollution Bulletin 135, 458-465.

Benjamin, A.M., Beasley, J.E., 2010. Metaheuristics for the waste collection vehicle routing problem with time windows, driver rest period, and multiple disposal facilities. Computers & Operations Research 37 (12), 2270-2280.

Bennett-Martin, P., Visaggi, C.C., Hawthorne, T.L., 2015. Mapping marine debris across coastal communities in Belize: developing a baseline for understanding the distribution of litter on beaches using geographic information systems. Environmental Monitoring Assessment 188 (10), 557.

Bergmann, M., Tekman, M.B., Gutow, L., 2017. Sea change for plastic pollution. Nature 544, 297.

California Ocean Science Trust, Oakland, CA., 2011. Plastic debris in the California marine ecosystem: a summary of current research, solution strategies and data gaps. 2011. C. Stevenson, University of Southern California Sea Grant. Synthetic Report.

Camedda, A., Marra, S., Matiddi, M., Massaro, G., Coppa, S., et al., 2014. Interaction between loggerhead sea turtles (Caretta caretta) and marine litter in Sardinia (Western Mediterranean Sea). Marine Environmental Research 100, 25-32.

Cordeau, J.-F., 2006. A branch-and-cut algorithm for the dial-a-ride problem. Operations Research 54(3), 573-586.

Cózar, A., Echevarría, F., González-Gordillo, J.I., Irigoien, X., Úbeda, B., et al., 2014. Plastic debris in the open ocean. Proceedings of the National Academy of Sciences 111 (28), 10239-10244.

Currie, J.J., Stack, S.H., McCordic, J.A., Kaufman, G.D., 2017. Quantifying the risk that marine debris poses to cetaceans in coastal waters of the 4-island region of Maui. Marine Pollution Bulletin 121, 69-77.

Demirel, E., Demirel, N., Gökçen, H., 2016. A mixed-integer linear programming model to optimize reverse logistics activities of end-of-life vehicles in Turkey. Journal of Cleaner Production 112 Part 3, 2101-2113.

Dias, B., 2016. Marine debris: understanding, preventing, and mitigating the significant adverse impacts on marine and coastal biodiversity. CBD Technical Series No.83. Secretariat of the Convention on Biological Diversity, Montreal, 78 pages.

Duan, G., Nur, F., Alizadeh, M., Ma, J. Marufuzzaman, M. 2019. Vessel routing and optimization for marine debris collection with consideration of carbon cap. Journal of Cleaner Production, 263, 121399.

GESAMP. 2015. Microplastics in the ocean: a global assessment, United Nations Joint Group of Experts on the Scientific Aspects of Marine Pollution. Working Group 40, gesamp.org.

Hauge, K., Larsen, J., Lusby, R.M., Krapper, E., 2014. A hybrid column generation approach for an industrial waste collection routing problem. Computers & Industrial Engineering 71, 10-20.

Hoffman, K.L., Padberg, M., 1993. Solving airline crew scheduling problems by branch-and-cut. Management Science 39 (6), 657-682.

Honorato-Zimmer, D., Kruse, K., Knickmeier, K., Weinmann, A., Hinojosa, I., et al., 2019. Inter-hemispherical shoreline surveys of anthropogenic marine debris - a binational citizen science project with schoolchildren. Marine Pollution Bulletin 138, 464-473.

Huang, S., Lin, P., 2015. Vehicle routing - scheduling for municipal waste collection system under the "Keep Trash off the Ground" policy. Omega 55, 24-37.

Jang, Y.C., Hong, S., Lee, J., Lee, M.J., Shim, W.J., 2014. Estimation of lost tourism revenue in Geoje Island from the 2011 marine debris pollution event in South Korea. Marine Pollution Bulletin 81 (1), 49-54.

Karamyar, F., Sadeghi, J., Yazdi, M.M., 2018. A Benders Decomposition for the Location allocation and Scheduling Model in a Healthcare System Regarding Robust Optimization. Neural Computing and Applications 29, 873-886.

Kizilates, G., Nuriyeva, F., 2013. On the Nearest Neighbor Algorithms for the Traveling Salesman Problem. Advances in Computational Science, Engineering and Information Technology 225, 111-118.

Landon-Lane, M., 2018. Corporate social responsibility in marine plastic debris governance. Marine Pollution Bulletin 127, 310-319.

Lavers, J.L., Oppel, S., Bond, A.L., 2016. Factors influencing the detection of beach plastic debris. Marine Environmental Research 119, 245-251.

Ma, J., Kremer, G., 2015. A Fuzzy Logic-Based Approach to Determine Product Component EOL Option from the Combination of Sustainability and Designer's Perception. Journal of Cleaner Production 108(Part A), 289-300.

Marine Mammal Commission, 1998. Annual Report to Congress. http://www.nmfs.noaa.gov/pr/readingrm/MMPAannual /1998_MMPA_Annual_Report.pdf Last Access:7/04/05.

Markov, I., Varone, S., and Bierlaire, M., 2016. Integrating a heterogeneous fixed fleet and a flexible assignment of destination depots in the waste collection VRP with intermediate facilities. Transportation Research Part B 84, 256-273.

Mascarenhas, R., Santos, R., Zeppelini, D., 2004. Plastic debris ingestion by sea turtle in Paraíba, Brazil. Marine Pollution Bulletin 49 (4), 354-355.

McIlgorm, A., Campbell, H., Rule, M., 2011. The economic cost and control of marine debris damage in the Asia-Pacific region. Ocean and Coastal Management 54 (9), 643-651.

Moy, K., Neilson, B., Chung, A., Meadows, A., Castrence, M., et al., 2018. Mapping coastal marine debris using aerial

imagery and spatial analysis. Marine Pollution Bulletin 132, 52-59.

Nowakowski, P., 2017. A proposal to improve e-waste collection efficiency in urban mining: Container loading and vehicle routing problems - A case study of Poland. Waste Management 60, 494-504.

Nowakowski, P., Król, A., Mrówczyńska, B., 2017. Supporting mobile WEEE collection on demand: A method for multi-criteria vehicle routing, loading and cost optimization. Waste Management 69, 377-392.

Nowakowski, P., Szwarc, K., Boryczka, U., 2018. Vehicle route planning in e-waste mobile collection on-demand supported by artificial intelligence algorithms. Transportation Research Part D 63, 1-22.

Oosterhuis, F., Papyrakis, E., Boteler, B., 2014. Economic instruments and marine litter control. Ocean & Coastal Management 102 Part A, 47-54.

Padberg, M., Rinaldi, G., 1991. A branch-and-cut algorithm for the resolution of large-scale symmetric traveling salesman problems. SIAM Review 33(1), 60-100.

Park, K., Kremer, G., Ma, J., 2018. A regional information-based multi-attribute and multi-objective decision-making approach for sustainable supplier selection and order allocation. Journal of Cleaner Production 187(20), 590-604.

Peng, X., Dasgupta, S., Zhong, G., Du, M., Xu, H., et al., 2019. Large debris dumps in the northern South China Sea. Marine Pollution Bulletin 142, 164-168.

Pisinger, D., Ropke, S., 2010. Large Neighborhood Search: Handbook of Metaheuristics. Springer, International Series on Operations Research and Management Science 146, 399-419.

Possatto, F.E., Barletta, M., Costa, M.F., Sul, J.A., Dantas, D.V., 2011. Plastic debris ingestion by marine catfish: an unexpected fisheries impact. Marine Pollution Bulletin 62 (5), 1098-1102.

Pritzker, P., Sullivan, K.D., Callender, R., 2015. Detecting Japan Tsunami Marine Debris at Sea: A Synthesis of Efforts and Lessons Learned. NOAA Technical Memorandum NOS-OR&R-51.

Ramos, T., Morais, C., Barbosa-Povoa, A., 2018. The smart waste collection routing problem: alternative operational management approaches. Expert Systems with Applications 103, 146-158.

Ropke S., Pisinger, D., 2006a. An Adaptive Large Neighborhood Search Heuristic for the Pickup and Delivery Problem with Time Windows. Transportation Science 40, 455- 472.

Ropke, S., Pisinger, D., 2006b. A Unified Heuristic for a Large Class of Vehicle Routing Problems with Backhauls. European Journal of Operational Research 171, 750-775.

Schulz, M., Walvoort, D., Barry, J., Fleet, D.M., van Loon, W., 2019. Baseline and power analyses for the assessment of beach litter reductions in the European OSPAR region. Environmental Pollution 248, 555-564.

Şebnem Düzgun, H., Onur Uşkay, S., Aksoy, A., 2016. Parallel hybrid genetic algorithm and GIS-based optimization for municipal solid waste collection routing. Journal of Computing in Civil Engineering 30 (3), 04015037.

Shaw, P. 1997. A New Local Search Algorithm Providing High-Quality Solutions to Vehicle Routing Problems. Technical Report, Dept of Computer Science, University of Strathclyde, Glasgow, Scotland, UK.

Sigler, M., 2014. The effects of plastic pollution on aquatic wildlife: current situations and future solutions. Water Air Soil & Pollution 225, 2184.

United Nations, 2017. 'Turn the tide on plastic' urges UN, as microplastics in the seas now outnumber stars in our galaxy. https://news.un.org/en/story/2017/02/552052-turn-tide-plastic-urges-un-microplastics-seas-now-outnumber-stars-our-galaxy.

van Sebille, E., Wilcox, C., Lebreton, L., Maximenko, N., Hardesty, B.D., et al., 2015. A global inventory of small floating plastic debris. Environment Research Letter, 10, 124006.

Vu, L., Tsun Wai Ng, K., Bolingbroke, D., 2018. Parameter interrelationships in a dual phase GIS-based municipal solid waste collection model. Waste Management 78, 258-270.

Wy, J., Kim, B.I., Kim, S., 2013. The rollon-rolloff waste collection vehicle routing problem with time windows. European Journal of Operational Research 224 (3), 466-476.

Yang, D., Shi, H., Li, L., Li, J., Jabeen, K., et al., 2015. Microplastic pollution in table salts from China. Environmental Science Technology 49, 13622-13627.

Zhang, H., 2017. Transport of microplastics in coastal seas. Estuarine, Coastal and Shelf Science 199, 74-86.